PROPOFOL MEDIATED CARDIOPROTECTIVE SIGNAL TRANSDUCTION: ETAR DEPENDENCE AND CAVEOLAR EFFECTS IN H9C2 CARDIOMYOBLASTS

by

Marijana Pavlovic

B.Sc., The University of British Columbia, 2013

A THESIS SUBMITTED IN PARTIAL FULFILLMENT OF

THE REQUIREMENTS FOR THE DEGREE OF

MASTER OF SCIENCE

in

THE FACULTY OF GRADUATE AND POSTDOCTORAL STUDIES

(Pharmacology and Therapeutics)

THE UNIVERSITY OF BRITISH COLUMBIA

(Vancouver)

September 2015

Abstract

Intro: Propofol is cardioprotective in the context of ischaemia-reperfusion. Components involved in propofol-mediated signaling involve AKT and STAT3. However, the involvement of the plasma membrane has not yet been elucidated. We hypothesized that propofol depends on two components located within the membrane — endothelin A receptor (ETAR) and caveolin.

Methods: H9c2 cardiomyoblasts were propofol-treated. To determine propofol-signaling dependence on ETAR, the selective ETAR inhibitor, PD156707 was used, and pSTAT3 Y705 protein levels were measured as a functional outcome. Similarly, caveolar-dependence was determined by disrupting cellular lipid rafts with methyl-β-cyclodextrin. ETAR – AKT interaction was explored via Co-IP. Immunocytochemistry was used to determine if propofol was affecting the cellular localization of ETAR, Cav-1, AKT, or Cav-3. Cav-1 cellular localization was also investigated using discontinuous sucrose gradient fractionation.

Results: Propofol-mediated-signaling (via pSTAT3 Y705 levels) was significantly reduced upon the inhibition of ETAR. In contrast, lipid raft disruption failed to reduce propofol-mediated-signaling. Propofol did not affect localization/ interaction of AKT. ETAR protein levels increased in intracellularly with propofol. Cav-1 protein expression/ localization did not change. However, Cav-3 levels did increase in the nuclear region with propofol treatment.

Conclusion: The results suggest that a component of propofol-signaling depends upon ETAR. Propofol signaling may act through a signalosome that involves receptor (ETAR) and Cav-3 internalization. This mechanism may be the avenue by which propofol is offering cardioprotection in a setting where other protection strategies are ineffective.

Preface

The author, M. Pavlovic, and Dr. Ansley designed the experiments. Dr. Bernatchez and Dr. Kumar provided input in design of specific experiments. M. Pavlovic performed the experiments and analyzed the data. This thesis presents unpublished, original work.

Table of Contents

List of Figures

List of Illustrations

List of Abbreviations

AKT	AKT
ATP	adenosine triphosphate
BAD	Bcl-2 associated death promoter
Bcl-2	B-cell lymphoma 2
BSA	bovine serum albumin
CABG	coronary artery bypass graft surgery
Cav-1	Caveolin-1
Cav-2	Caveolin-2
Cav-3	Caveolin-3
CHO	Chinese hamster ovaries
CO_2	carbon dioxide
Co-IP	co-immunoprecipitation
Cy	cyanine
DAMPS	damage-associated molecular patterns
DMEM	Dulbecco's modified Eagle's medium
DMPC	dimyristoyl-L-α phosphatidylcholine
DMSO	dimethylsulfoxide
DNA-PK	DNA-dependent protein kinase
DPBS	Dulbecco's phosphate buffered saline
DPPC	dipalmitoyl phosphatidyl choline
EDTA	ethylenediaminetetraacetic acid

EGFR	epidermal growth factor receptor
EGTA	ethylene glycol tetraacetic acid
eNOS	endothelial nitric oxide synthase
ERK	extracellular signal-regulated kinase
ET-1	endothelin 1
ETAR/ ETBR	endothelin receptor A/ B
FBS	fetal bovine serum
FITC	fluorescein
HSD	honest significant difference
HO•	hydroxyl radical
HUVEC	human umbilical vein endothelial cells
IR	insulin receptor
JAK2	janus kinase 2
MAPK	mitogen-activated protein kinase
MBS	MES buffered saline
MES	2-(N-Morpholino)ethanesulfonic acid
mPT	membrane permeability transition
mPTP	membrane permeability transition pore
mTOR	mammalian target of rapamycin
NFκB	nuclear factor kappa-light-chain-enhancer of activated B cells
NO	nitric oxide
NO•	nitric oxide radical

O_2•	superoxide
PAGE	polyacrylamide gel electrophoresis
PDK1	3-phosphoinositide-dependent protein kinase 1
PI3K	phosphoinositide 3-kinase
PIP2	phosphatidylinositol (3,4)-bisphosphate
PIP3	phosphatidylinositol (3,4,5)-trisphosphate
PKC	protein kinase C
PMSF	phenylmethylsulfonylfluoride
pSTAT3	phosphorylated STAT3
PTEN	phosphatase and tensin homologue on chromosome 10
RISK	reperfusion injury salvage kinase
RPM	revolutions per minute
S727	serine 727
SAFE	survivor activating factor enhancement
SD	standard deviation
SDS	sodium dodecyl sulphate
SH2	src homology 2
siRNA	small interfering RNA
STAT3	signal transducer and activator of transcription 3
TNFα	tumor necrosis factor α
TGFβ	transforming growth factor beta
Y705	tyrosine 705

Acknowledgements

I sincerely thank my supervisor, **Dr. Ansley**, for the support, guidance, and the push to become a better scientist during my master's degree. Additionally, I would like to thank my co-supervisor, **Dr. Bernatchez**, for his guidance and advice during this degree, especially in the realm of caveolae. I would sincerely like to thank **Dr. Kumar** for his guidance and advice for my project. Immunofluorescence and Co-IP experiments were done in the laboratory of Dr. Kumar, as was Western blot development. I would also like to thank **Dr. Molday**, as a member of my supervisory committee. I also thank, **Dr. Rishi Somvanshi** for his technical help, and many useful conversations. Ultracentrifugation of discontinuous sucrose gradients was performed in the laboratory of **Dr. Naus.** I would like to thank **Maxence LeVasseur**, and **Andy Trane** for their technical help with the ultracentrifugation. I offer my gratitude to **Dr. Baohua Wang**. Although, only present during the first couple months of my master's degree, Dr. Wang helped me set up strong technical groundwork. My project has been funded by the Canadian Anesthesiologists' Society/ Canadian Anesthesia Research Foundation and Canadian Institute of Health Research.

I am also grateful to the staff and graduate students of the Department of Anesthesiology, Pharmacology and Therapeutics, as well as members of the Bernatchez lab at the Heart and Lung Institute of St. Paul's and members of the Kumar lab in the Pharmaceutical Sciences Department. Special thanks to my family and friends, for their support in everything, including this endeavor.

Dedication

For my family, especially my parents — for all the support, encouragement, and understanding.

Chapter 1: Introduction

1.1 Scope

Beyond its actions as a general anesthetic, propofol affects the physical and signaling properties of membranes. These phenomena have not been fully explored. Furthermore, in propofol's ability to mitigate ischaemia-reperfusion injury, certain membrane components are implicated, but not fully elucidated. Thus, this thesis investigates the potential involvement and role of the membrane components endothelin A receptor (ETAR) and caveolae, in cardioprotective propofol-mediated-signaling.

1.2 Part I

1.2.1 Lipid membranes

The cellular membrane, a lipid bilayer, encloses and protects the cell. Its primary lipid constituents are amphipathic phospholipids — consisting of a polar, hydrophilic phosphorylated head group, and a double hydrophobic fatty acid tail [1]. The polar head groups face the extracellular matrix, and the intracellular cytosol [1]. The hydrophobic tails associate with each other, and are thus segregated from the aqueous environments mainly due to entropic considerations [2]. Numerous varieties of phospholipids are present, differing in abundance based on leaflet (inner/outer) as well as cell type [3,4]. Phospholipids differ by phosphorylated head group (e.g. choline vs. serine) and hydrophobic lipid tail group (acyl

chain length/ number of double bonds) [1]. A host of other moieties are found within the cellular membrane — other lipids (such as sphingolipids and sterols) as well as proteins [4]. Initially all of these components were thought to exist in a homogenous randomized sea — Singer and Nicolson's fluid mosaic model [2].

1.2.2 Lipid rafts (structure)

Although Singer and Nicolson's fluid mosaic model took into account hydrophobic and hydrophilic energy considerations [2], the cellular biological membrane is also organized at a higher level [5–7].

Once one moves beyond the study of model membranes and systems, or even creates a simpler heterogeneous model system, the lipids start differentially organizing into phases [8–10]. Pockets of lipid microenvironments exist within the membrane that can be loosely categorized based on the lipid fluidity [11]. There are three main membrane lipid organizations ranging from least to most rigid — liquid disordered/liquid crystalline, liquid ordered, and gel [1,6,11]. Phase identity of microdomains depends on the lipid composition, as well as on the temperature [1,12,13]. Furthermore, the phase transition temperature varies between different cell types, as their lipid abundance compositions vary [1]. The gel phase, of phospholipid membranes occurs at low temperatures and the phospholipids are packed rigidly, with little room for motion [1]. At higher temperatures phospholipid membranes can be found in the liquid disordered state — where they are not packed as tightly and have a greater freedom of motion [1]. The addition of cholesterol to membranes introduces the third type of phase —

liquid ordered, which is an intermediate between the liquid disordered and the gel phases [1]. Thus in model membranes, control of the amount of cholesterol and temperature, can control the phases that occur in the membrane [1,12].

Lipid rafts are in the liquid ordered state, surrounded by a liquid disordered state [6,11,12]. They are enriched in cholesterol and sphingolipids (such as ceramides, sphingomyelin, and glycosphingolipids) [5,6]. Additionally, they also have a slightly higher percentage of saturated phospholipids [6]. Lipid raft rigidity in relation to its surroundings, comes from the tight packing of saturated phospholipid tails, sphingolipid acyl chains, and cholesterol [1]. The composition varies with cell type — Sonnino et al. (2007) reported the mol% composition of rat cerebellar granule cells as being roughly 55 for phospholipids, 25 for cholesterol, 20 for sphingolipids, and < 0.5 for proteins [7]. Additionally, there is a greater abundance of gangliosides present in neural cell lipid rafts [6].

Cholesterol is an integral part of the lipid rafts. Without cholesterol, lipid rafts would not exist. For one, in membrane models, the lipid raft liquid ordered phase is absent until the addition of cholesterol, even in the presence of phospholipids and sphingolipids (although there have been some reports about the ability of sphingolipids to cluster and self-organize together) [1,7]. Furthermore, in biological membranes, if cellular cholesterol is depleted via a number of ways (for example with the addition of statins or methyl-β-cyclodextrin), the lipid rafts are disrupted, non-functional, and absent [14].

The sphingolipids with large sugar head groups (glycolipids/ gangliosides) induce a positive curvature [7]. The larger the attached sugar moiety, the larger the induced curvature [7]. This property is especially useful when it comes to forming continuity between the negative curvature induced by caveolae and the rest of the cellular membrane [7].

The cellular cytoskeleton is important for the structure and organization of lipid rafts. Numerous proteins found within lipid rafts such as ezrin associate with actin [15,16]. The actin cytoskeleton is responsible (at least in part) for remodeling the location of lipid rafts — e.g. for helping them conglomerate into larger rafts [15–17].

1.2.3 Caveolae

Caveolae are a subtype of lipid rafts. There are two main distinguishing features of caveolae — they possess the scaffolding protein caveolin and they have a negative membrane curvature [16,18–21]. The negative curvature joins via the rest of the membrane via a positive curvature induced by the sphingolipids — the larger the group attached to the head, the more pronounced the curvature [7]. These 50-100nm invaginations were initially observed and documented by Palade (1953) [22]. Palade (1953) described what he viewed as ~650Å vesicles which open up into extracellular space in the endothelium [22]. Whereas Yamada (1955) shortly afterwards described them in the mouse gall bladder epithelium and gave them the name — *caveolae intracellularis* — or shortened to caveolae [23]. The scaffolding protein caveolin inserts into the membrane, forming a loop, with both termini located in the cytoplasm [16,19].

The precursors of caveolae are formed initially in the endoplasmic reticulum — caveolins, cholesterol, and sphingolipids [16,19]. Initial caveolin oligomerization occurs at this stage as well, although the final high molecular weight oligomers are not yet achieved [16,19]. The precursors are then shuttled to the Golgi apparatus where they assemble [16,19]. Additionally, caveolin has its cysteine palmitoylated [16]. Then they are shuttled to the cell surface with the help of microtubules [24]. In the absence of sphingolipids caveolin are unable to evacuate the Golgi apparatus [19].

There are three structural isoforms of caveolin — Caveolin-1 (Cav-1), Caveolin-2 (Cav-2), and Caveolin-3 (Cav-3) [16,18,19]. Isoform type, interaction, and abundance, depends on the cell type [18]. Generally it has been described that Cav-3 presents in striated muscle cells (cardiac and skeletal) and Cav-1/Cav-2 presents in other cell types — such as the endothelium, adipocytes, etc. [16,19,25]. However, there are caveats to this simplified categorization. For one, there are cell types that possess all three isoforms of caveolin — such as cardiomyocytes and aortic smooth muscle cells [17,26]. Additionally, non-cardiac cells including neuronal cells (which do not express the caveolae organelle), glial cells, and bladder smooth muscle cells possess all three isoforms of caveolin [27,28]. Aside from expressing all three isoforms of caveolin, all three caveolin isoforms interact in adult cardiomyocytes [17]. However, there are cell types that contain all three isoforms and only two interact [25]. In cells that express all three isoforms, levels of individual caveolin isoforms may change in different environments[27].

Caveolins self-assemble into higher weight hetero/homo oligomers (for example, Cav-1/Cav-2 heteroligomers consists of 12-18 monomers, Cav-3 homoligomers consist of 9 monomers, Cav-1 homoligomers >14 monomers) [16,27,29]. However, Cav-1/Cav-2/Cav-3 heteroligomers (although tissue specific) are also possible, as are Cav-2/Cav-3 heteroligomers [18,28].

Caveolin is necessary and sufficient for the formation of caveolae (with some caveats) [19]. Certain neural cells possess all three isoforms of caveolin, and yet have no discernable caveolar structures [16,27]. Additionally, overexpression of Cav-1/Cav-3 enhances the formation of caveolae [19,30,31]. Conversely, knocking out caveolin eliminates the caveolae structure (except for Cav-2, whose deletion does not result in disruption of caveolae) [19].

Caveolins contain a scaffolding domain which interacts with many proteins, such as endothelial nitric oxide synthase (eNOS), insulin receptor (IR), epidermal growth factor receptor (EGFR), and endothelin receptors (ETAR/ETBR) [6,32]. Beyond interaction, the caveolin scaffolding domain has the ability to regulate some of these moieties — for example, it is a positive modular of IR, and a negative modulator of eNOS [32,33].

Caveolae, like its higher categorization, lipid rafts, interact with cytoskeletal elements — namely through caveolin [27]. Stalhut and van Deaurs (2000) demonstrated that there is a link between actin and caveolae — filamin is present in caveolae and it interacts with Cav-1 [29]. Actin is necessary for caveolae's endocytic ability [34,35]. Additionally, intact actin seems to be essential for proper caveolae developments — as disrupting it leads to decreases in Cav-1.

Cav-2 and Cav-3 in light, lipid raft fractions [17]. Microtubules are also essential for caveolar endocytic trafficking [24].

1.2.4 Lipid rafts and caveolae (signaling)

Within lipid rafts a variety of cell-signaling molecules congregate [5,6,20]. For example, many cell signaling receptors are located within lipid rafts — both the tyrosine kinase and G-protein coupled variety [6,33]. It is widely believed that lipid rafts, and caveolae are important in cellular signaling [6]. For one, it provides an avenue via which signaling moieties are within close proximity to each other [6].

Lipid rafts are a dynamic system, with receptors and proteins having the ability to translocate to and from these rafts. They are also involved in endocytosis. Caveolae, especially, offer a clathrin-independent type of endocytosis [36]. This route is taken advantage of by some viruses, as it is able to bypass vesicle maturation to lysosomes and subsequent degradation [36]. Endocytosis through caveolae is also a promising route of delivery for nanomedicine [36].

As aforementioned, caveolin has a C-terminal scaffolding domain (CSD) which interacts with proteins, modulating them. Aside from this interaction, modifications to proteins such as palmitoylation, myristoylation, and sumoylation help increase the affinity of proteins to lipid rafts [16].

1.2.5 Propofol

Propofol (2,6-diisopropylphenol) is an intravenous general anesthetic. The molecule is highly hydrophobic, which is aided, in part, by the steric hindrance of the ortho-substituted propyl groups (which restrict access to the phenolic hydroxyl group). Furthermore, the phenolic group's ability to resonance stabilize a charge, confers propofol antioxidant capabilities. The compound, 2,6-diisopropylphenol, patented by Ecke and Kolka in 1966, was initially intended to be an adjunct for polymers and oils in order to prevent undesirable oxidation [37]. Subsequently, in 1975, John Baird Glen and Roger James filed a patent for the use of 2,6-diisopropyl phenol as an intravenous anesthetic [38]. James and Glen (1980) assessed the anesthetic potential of a series of alkylphenols, and discovered that 2,6-diisopropylphenol was the most potent [39]. Initially, propofol was preferentially administered with Cremaphor® (a castor oil derivative) [38,40]. However, this formulation was associated with an elevated incidence of anaphylactic shock, and propofol was reformulated with a lipid emulsion (Intralipid ®) [41,42]. Intralipid ® alone induces biological (non-anesthetic) activity [43,44].

1.2.6 Propofol's effects on lipid membranes — Biophysical properties, and effects on model membrane systems

Propofol's effects on the biophysical properties and integrity of lipid membrane have been investigated via experiments (from model membrane systems to erythrocytes) and simulations. Overall, propofol has been found to have a fluidizing effect on lipid membranes.

However, the experimental conditions (e.g. temperature and concentration) vary between the studies, and could be responsible for variances in results.

In uniform dimyristoyl-L-α phosphatidylcholine (DMPC) models it was found that in the gel-phase, near the gel-fluid phase transition temperature, propofol decreased viscosity and increased fluidity in concentrations equal to or greater than 10^{-4}M [45]. At temperatures significantly higher than the gel to fluid phase transition critical temperature, Bahri et al (2007) found that propofol had no effect on membrane fluidity [45]. Balasubramian et al (2002) used a different liposome — containing dipalmitoyl phosphatidyl choline (DPPC) – and also found that slightly below the gel-fluid transition temperature, propofol (0.5μM) had the effect of fluidizing the membrane [46]. Of note, however, is that there was an effect seen at 0.5μM, whereas Bahri et al (2007) needed drastically higher concentrations. Balasubramian et al. (2002) also found that propofol at that concentration had no fluidizing effect at temperatures significantly above or below the gel-fluid phase transition temperature. Moreover, not only does propofol have a fluidizing effect at this near gel-fluid phase transition temperature, but it also promotes the formation of separate fluid domains [46]. Tsuchiya (2001) also noted propofol fluidizing effects in the micromolar range on single lipid model liposomes, including DPPC as well as mixed-lipid liposomes with the addition of cholesterol [47]. The presence of propofol lowers the critical temperature of the gel-fluid transition in both DMPC and DPPC liposomes, but there is a discrepancy in the literature as to the concentration of propofol required [47,48].

Propofol's ordering effects on membrane structure is similar to that of phenol, but more pronounced [48]. Its ordering effect has also been compared to that of cholesterol [49].

Propofol associates with lipid bilayers. Propofol is highly hydrophobic — it has an octanol-water partition coefficient of 2.84 [48]. Although it has the polar hydroxyl group, it is blocked and shielded by the two isopropyl groups. Propofol's association with lipid membranes is thus highly favourable. Simulations and investigations with model liposomes showed that propofol is located on both sides of the lipid bilayer, near the lipid head group (where its hydroxyl group can hydrogen bond with the glycerol backbone) [45,47,49]. Although some useful information can be gathered from these model systems, the real lipid membrane behaves quite differently – due to many different types of lipids and proteins present. Phase transition temperatures vary drastically between cell types, if at all even present, and the types of lipids present [50]. Even within the same cell type, the ratio of lipids present is a dynamic, changing, process.

It is also important to note that at certain concentrations, propofol has damaging effects on lipid membranes [45]. Bahri et al (2007) found that concentrations under 10^{-4}M did not invoke any cytotoxic effects [45]. However, values of 10^{-3}M and greater started inducing erythrocyte lysis [45].

1.2.7 Propofol and lipid rafts/caveolae

Much less work has been done on the exploration of the effect of propofol on lipid rafts/ caveolae. Moving beyond the DPPC and DMPC liposomes with/without cholesterol, model lipid raft systems include liposomes made up of equal parts 1-palmitoyl-2-oleoyl-sn-glycero-3-phosphocholine, sphingomyelin and cholesterol, as well as giant plasma membrane vesicles that contain both a liquid ordered and disordered phase [51,52]. In both of these models the critical temperature for phase transition is lowered by a couple of degrees with the addition of propofol [51,52]. No other major propofol-induced structural changes to lipid rafts have been reported [51,52].

One study looked at the effect of propofol on caveolae at a biological level. Grim and colleagues (2012) investigated ultimately the dependence of propofol-mediated bronchodilation on caveolae [53]. They found that upon propofol treatment, elevated levels of propofol were retained in caveolar regions of the membrane [53]. Additionally, there was a decreased intracellular calcium ion content response to a variety of stimuli including acute caffeine and histamine application in the presence of propofol — an effect which was abolished when caveolae were disrupted with small interfering RNA (siRNA) [53].

Overall, the field of research into the effects of propofol on caveolae, or even lipid rafts is still in its nascent stages. Further work is required to fully elucidate the interaction between caveolae and propofol.

1.3 Part II

1.3.1 Ischaemia-reperfusion injury

When tissue experiences a decrease in blood perfusion (ischaemia), and subsequent reintroduction of blood (reperfusion), it is susceptible to ischaemia-reperfusion injury [54–56]. It is not solely the ischaemic period which induces the damage (although longer periods of occlusion correlate with greater levels of subsequent damage), but also the reperfusion [55–57]. Moreover the area of damage of a single long extended period of ischaemia is equivalent to a much shorter ischaemic period coupled to a reperfusion [57,58]. Reperfusion speeds up the cell death process that initiated with ischaemia in the area of injury, as well as contributing to additional surrounding injury [57,59]. All tissues are potentially vulnerable to ischaemia-reperfusion injury, including the heart.

In cardiac tissue there are a number of changes that occur in response to ischaemia-reperfusion. Upon the reduction of blood flow, logically oxygen levels drop, and carbon dioxide levels rise, coupled with a decrease of adenosine triphosphate (ATP) as oxygen becomes scarce [56]. A shift in in cellular metabolism occurs in favour of non-oxygen consuming energy generation (glycolysis), and one of the results is lowering of intracellular pH [55]. Cells undergo massive amounts of oxidative damage from reactive oxygen species (ROS) and reactive oxidative nitrogenous species (RONS) that are generated in the process [60]. This generation is multifaceted, occurring from various sources [56]. Keynote radicals generated include superoxide (O_2•), hydroxyl radical (HO•), nitric oxide (NO•) [60].

Although, radical generation commences in the ischaemic stage, the greatest free radical production and propagation occurs upon reperfusion [55,56]. The radicals cause a range of damage, including lipid peroxidation, and can lead to the activation of the membrane permeability transition (mPT). The mPT leads to the opening of the membrane permeability transition pore (mPTP) [56]. Once mPTP occurs, the cell has started its transition towards death — either via necrosis or apoptosis (which largely depends on the remaining cellular energy levels) [56]. Aside from the oxidative stress inducing mPTP, reperfusion following ischaemia sets the stage in other ways for mPTP. The return of cellular pH to physiological levels causes an ionic imbalance that the cell corrects for by increasing calcium ion levels [55,56]. A calcium overload in turn promotes the formation of mPTP [55,56]. Oxidative stress and large increases in intracellular calcium lead to the formation of mPTP and consequently cell death – apoptosis, necrosis, and potential autophagic cell death [55,56,61].

The damage permeating to the cellular level is multifaceted. Massive amounts of cell death are occurring through apoptotic (programmed cell death, involving caspases and B-cell lymphoma 2 (Bcl-2) family members), necrotic (non-programmed cell death) and/or autophagic (self-digesting) mechanisms [54,62]. Additionally, necrosis can further be split into two pathways: structured (necroptosis), where the cell maintains some control of the process, and unstructured, where the contents of the cytoplasm are spilled into the extracellular matrix indiscriminately [62]. Inhibiting autophagy lessens injury to a certain extent, even though protective benefits of autophagy have also been reported [61,63,64]. Interestingly, autophagy and apoptosis counter-regulate each other [61,64]. Depending on experimental parameters, various studies have found different ratios of apoptotic: necrotic cells as a result of ischaemia-

reperfusion injury. (As of yet, there are no studies that directly looked at proportion of apoptotic: two different necrotic subtypes: autophagy). Kajstura et al., (1996) found that the number of apoptotic cells vastly outnumber (6:1) necrotic cell death, and that apoptosis is initiated earlier [65]. It is a possibility that in the earlier stages of the injury, when the damage is not as extensive, that there is sufficient energy available to undergo apoptosis. However, the balance may shift to necrosis in the late stages. On the other hand, Linkerman et al. (2013) suggested that necrosis has a much bigger role as compared to apoptosis in the extent of ischaemia-reperfusion damage [62]. If the process of necroptosis is inhibited by either pharmaceuticals (which incidentally also prevent apoptosis) or knockout mice models of a key pathway player, ischaemia and reperfusion injury is drastically decreased [62].

Inflammation and immune system response elements are recruited to the infarct site. Cells undergoing damage (such as oxidative damage) and necrosis release chemoattractants (damage-associated molecular patterns (DAMPs)), which act to recruit neutrophils to the infarct site [54,55,59]. Moreover, apoptosis also activates the immune system by attracting phagocytes [54]. Inflammatory mediators are also recruited to site, and exacerbate the injury [54,55]. Although there is some benefit from certain elements of the immune system, the overall effect on injury is deleterious [54,55].

Aside from cell death, and recruitment of the immune system, ischaemia-reperfusion injury in the myocardium and vascular system causes many other perturbations that are not conducive to normal, healthy cellular and tissue function [54]. At the level of the vasculature, ischaemia-reperfusion injury leads to endothelial dysfunction which in turn exacerbates

vascular permeability, and an imbalance of vasoconstrictors [54]. Abnormal platelet aggregation is also present [54,66]. Finally, as far as the vasculature is concerned, there is also an incidence of "no-reflow" phenomenon, where even upon reperfusion not all of the vasculature immediately experience reflow [54]. Subsequently, the heart organ itself is prone to arrhythmias, contractile function abnormalities, and stunning [56,57].

1.3.2 Ischaemia-reperfusion injury: Coronary artery bypass graft surgery

Ischaemic episodes (which may be followed by reperfusion) can occur due to a variety of different natural causes, including atherosclerotic vascular disease, blood clot, or acute injury. As a result, surrounding tissue is susceptible to ischaemia-reperfusion injury [54]. However, during cardiac surgery the heart is prone to ischaemia-reperfusion injury. When undergoing cardiopulmonary bypass blood flow to the heart is temporarily interrupted. Afterwards, blood is reperfused, paving the way for potential ischaemia-reperfusion injury [56]. Ischaemia-reperfusion injury, in this surgical context, can lead to numerous negative morbidities, such as low cardiac output syndrome, poor ventricular function, arrhythmias, myocardial infarction and even acute heart failure; at their most severe these may lead to death [54,67]. Certain subsets of the population, including people with diabetes are even more susceptible to ischaemia-reperfusion injury than the general population [60].

The level of cardiac injury following CABG in patients may be assessed/ monitored in a number of different ways. One way is the quantification of injury-associated biomarkers in

blood. These include, troponin I, lactate dehydrogenase, and creatine kinase levels [68]. Echocardiography and hemodynamic monitoring may also be used [66,69].

1.3.3 Ischaemia-reperfusion injury and propofol

Propofol has been documented to experimentally decrease ischaemia-reperfusion injury in a variety of organs, including brain, intestine, lung, liver, kidney and heart [67,70–76]. In studies of its cardioprotective potential, propofol has been shown to mitigate the damage from ischaemia-reperfusion injury in a variety of cell models, isolated heart models, and low risk patients.

In endothelial and cardiomyocyte cell culture cell models propofol helps prevent ischaemia-reperfusion damage related cell death (namely inflammatory and oxidative damage) [77–79]. Human umbilical vein endothelial cells (HUVEC) show reduced apoptosis and increased antiapoptotic markers when treated with propofol as compared to a control in the face of oxidative damage (H_2O_2) or inflammatory (tumor necrosis factor α (TNFα)) [77,78]. Likewise, H9c2 (embryonic rat cardiomyoblast cells) show increased resistance to apoptotic cell death against hydrogen peroxide injury when treated with propofol [79].

Langendorff isolated animal hearts (rat, guinea pig, and rabbit) perfused with propofol before and/ or during experimentally-induced ischaemia-reperfusion had decreased indices of injury[74,80–82]. These effects are not limited to adult models, but also extend from juvenile to middle aged models [74,82]. Lim et al. (2005) used a relevant CABG surgery model with pigs,

and treated the hearts with propofol both prior to and during the ischaemic episode [69]. They found that biomarkers associated with damage were decreased and haemodynamic dysfunction reduced with propofol treatment. Additionally, end levels of ATP in the propofol condition were statistically higher than in the control [69].

One of the advantageous effects of propofol use in the context of curbing ischaemia-reperfusion injury is the associated decrease in oxidative damage [73,74]. In a study that compared the continuous infusion of propofol versus isoflurane in patients undergoing elective CABG, a high dose of propofol decreased plasma levels of malondialdehyde, a marker of oxidative stress [83]. Furthermore, in vivo, a high propofol dose diminished cardiac damage, as demonstrated by lowered levels of cardiac injury biomarkers (troponin I and creatine kinases), and improved postoperative cardiac indices and systematic vascular resistance [83].

Taken together, these studies indicate the cardioprotective potential of propofol to alleviate clinically relevant ischaemia-reperfusion injury, and its sequelae.

1.3.4 Preconditioning

Fortunately, protective strategies (pre and post conditioning) that offer evidence of protection against ischaemia-reperfusion injury have been empirically documented. Preconditioning strategies can be divided into three broad categories — ischaemic conditioning (and the

subtype — remote ischaemic conditioning), and pharmacologic conditioning (and its subtype — volatile anesthetic conditioning).

During ischaemic conditioning brief periods of occlusion help prime and protect the heart from a subsequent longer period of ischaemia-reperfusion [56,84]. Murry et al. (1986) first described the phenomena of ischaemic preconditioning [84]. The authors documented that a brief series of regional coronary artery occlusions prior to index ischaemia, mitigated indices of cardiac injury, (reduced infarct size as compared to control), in a dog model. Since then, research has rapidly expanded, been reproduced in many other animals (and organ systems), and translated into small clinical studies – showing benefit in the mitigation of ischaemia-reperfusion injury [85–87].

Subsequently, the principles of ischaemic postconditioning and remote ischaemic conditioning were developed. Ischaemic postconditioning involves brief artery occlusions following an ischaemia-reperfusion event, such as a myocardial infarction [55,88,89]. Zhao et al. (2003) were the first to document postconditioning as a technique with comparable benefits to preconditioning [89]. Alternatively, remote ischaemic conditioning confers cardioprotection through brief pulsed ischaemic episodes prior to index ischaemia in a remote organ or limb[55,90–92].

Although beneficial, ischaemic conditioning techniques remain imperfect. For example, the repeated occlusions involved in ischaemic preconditioning stress the vasculature[55]. Furthermore, particular sub-populations (e.g. patients with diabetes) that possess an elevated

risk of ischaemia-reperfusion injury, are resistant to the protective effects of ischaemic conditioning. [60].

Pharmacologic conditioning invokes, to varying degrees of success, pharmacological strategies for amelioration and/or prevention of ischaemia-reperfusion injury. Some were specifically chosen to address direct damage caused by ischaemia-reperfusion — be they anti-inflammatory, or antioxidants (including propofol), or whether they conferred other overall protective effects to the damaged myocardium. Examples of such agents include K_{ATP} channel openers (e.g. Nicorandil), adenosine receptors agonists (e.g. adenosine and IB-MECA), sodium/ hydrogen exchange inhibitors (e.g. Ethyl-isopropyl-amiloride), mPTP pore inhibitors (e.g. cyclosporine) as well as nitric oxide donors [93]. Furthermore, volatile anesthetics were also investigated as potential positive mediators of ischaemic damage. These anesthetics included sevoflurane, halothane, and isoflurane [94].

1.3.5 Protective pathways activated in preconditioning: Overview

Ischaemic preconditioning activates a series of protective pathways which culminate in the preservation of mitochondrial membrane integrity (inhibition of mPTP) and consequently, a prevention of cellular death [95]. This effect is shared by pharmacological preconditioning activates components of these common pathways as well.

Both individual and synchronous activation of pathways has been documented in conditioning [96]. Furthermore, the protective pathways can also be inherently linked through a

crosstalk mechanism, and disturbing one pathway will arrest any form of protection occurring [96,97].

Preconditioning activates a cascade of cell signaling pathways which culminate in promoting cell survival. Activated pathways include the reperfusion injury salvage kinase (RISK) pathway as well as the survivor activating factor enhancement (SAFE) pathway.

1.3.6 Protective pathways activated in preconditioning: RISK pathway

A crucial component of RISK, is the phosphoinositide 3-kinase (PI3K)/ AKT pathway. PI3K adds a phosphate group to phosphatidylinositol (3,4)-bisphosphate (PIP_2), converting it to phosphatidylinositol (3,4,5)-trisphosphate (PIP_3) This step can be inhibited by phosphatase and tensin homologue on chromosome 10 (PTEN) [98]. AKT localizes to the cellular membrane, associating with PIP3, where it is phosphorylated by 3-phosphoinositide-dependent protein kinase 1 (PDK1) on threonine 308 [98]. Although AKT is now partially active, AKT is not fully active until its other phosphorylation site — serine 473 is phosphorylated by either mTOR or DNA-dependent protein kinase (DNA-PK) [98]. AKT has a host of cellular downstream factors which it can subsequently activate [98]. Especially important to the concept of preconditioning to counter ischaemia-reperfusion damage is AKT's role in cell proliferation and cell survival [98]. For example, AKT is involved in inhibition of Bcl-2 associated death promoter (BAD), in activation of eNOS to produce nitric oxide (NO), activation of extracellular signal-regulated kinase (ERK) 1/2 [68,95,98,99].

1.3.7 Propofol's effect on the RISK pathway

Propofol activates components of the RISK pathway, resulting in in vitro cellular protection. However, certain components are differentially activated depending on cell type. In cardiomyoblasts, propofol upregulates activated (phosphorylated) AKT levels, as well as pro-survival Bcl-2 levels in the presence of pro-apoptotic stimuli [79]. Although endothelial cell Bcl-2 experiences a similar response to propofol, a response recapitulation of phosphorylated AKT levels is lacking [77,78,100]. (Neurons, conversely also experience increases of phosphorylated AKT in response to propofol treatment [101]). However propofol does increase eNOS activity, and consequently NO production in endothelial cells [77,78,100]. Moreover, propofol also influences differential cellular distribution of a protein kinase C (PKC) isoform in endothelial cells [100]. Ultimately propofol protects, through a partially RISK-dependent pathway, both endothelial (HUVEC) and cardiomyoblast (H9c2) cells from apoptosis in a simulated ischaemia-reperfusion model [77,79].

1.3.8 Protective pathways activated in preconditioning: SAFE pathway

Signal transducer and activator of transcription 3 (STAT3) is an important component of the SAFE pathway. Receptor dimerization promotes the binding of janus kinase 2 (JAK2) via its homologous domain [102]. JAK2 in turn phosphorylates STAT3 (which also docks at the receptor via its src homology 2 (SH2) domain) [102]. STAT3 can be phosphorylated on tyrosine 705 (Y705) or serine 727 (S727) [103,104]. STAT3 has the ability to translocate to the nucleus[104]. This translocation was originally viewed to be pSTAT3 Y705 dependent [104].

However, the translocation process is a dynamic one occurring basally at all times [104]. Phosphorylation of STAT3 Y705 does induce dimerization on the other hand, which allows STAT3 to recognize a consensus DNA sequence and act as a transcription factor [104,105]. STAT3 is a transcription factor for many genes required for cell growth and proliferation, including the anti-apoptotic Bcl-2 [104,105].

Phosphorylation of STAT3 on the serine moiety in contrast activates a different set of pathways. Phosphorylated STAT3 serine is found in the mitochondria — where it helps to maintain and support the electron transport chain (mitochondrial oxidation) [103] .

1.3.9 Propofol's effect on the SAFE pathway

In addition to affecting the RISK pathway, propofol also affects the SAFE pathway. Propofol application upregulates STAT3 phosphorylation (Y705 and S727) [97]. Furthermore, Bcl-2, a putative effector of both aforementioned signaling pathways is increased with propofol treatment [97]. Additionally, propofol treatment increases STAT3 localization in the nucleus of the cell [97].

1.3.10 Interaction between the RISK and SAFE pathways

To a certain extent there is codependence between the RISK and the SAFE pathways in preconditioning. However, there are exceptions to this generalization. Experimentally, when STAT3 is knocked out or inhibited, ischaemic preconditioning is nonexistent [95,96]. Likewise,

ischaemic preconditioning is abolished with AKT inhibition [96]. However, small amounts of TNFα induce preconditioning solely through the SAFE pathway [95,96].

Previous work in our laboratory has shown that RISK-SAFE pathway cross-talk is essential to propofol-mediated signaling [97]. As previously mentioned and reported, propofol activates components of both the RISK and SAFE pathways through phosphorylation, namely AKT, and STAT3 respectively [77,79,97]. When either of these pathways are inhibited, the other one suffers a loss of propofol mediated signaling (i.e. activation/ phosphorylation) [97]. Thus when either JAK2 or STAT3 (from the SAFE pathway) is inhibited, there is a corresponding decrease in AKT phosphorylation in response to propofol [97]. Conversely when PI3K or AKT (from the RISK pathway) is inhibited, there is a corresponding loss of STAT3 phosphorylation (from the SAFE pathway) in response to propofol [97].

Thus propofol signaling is dependent on the crosstalk between the RISK and the SAFE pathways — a pattern it shares with certain examples of ischaemic preconditioning. This is to emphasize the parallels that are already evident between ischaemic preconditioning, and propofol's cardioprotective signaling effects.

1.3.11 Caveolins and ischaemia-reperfusion injury

Ischaemia-reperfusion (as well as certain other types of heart disease) affects caveolae. Overall, cardiac caveolin presence seems to be protective, possibly due to the positive modulatory effect on the RISK and SAFE pathways.

Ischaemia-reperfusion injury downregulates Cav-1, and redistributes Cav-3 to the cytosol[18,106]. Additional caveolar decreases of Cav-3 occur in catecholamine induced hypertrophy [107].

Caveolin presence has documented cardioprotective ramifications, especially in the context of ischaemia-reperfusion injury. In general, knockout caveolin mouse models have poor cardiac function [18]. Additionally, knockout models of either Cav-1, Cav-3, or both, exhibit exacerbated ischaemia-reperfusion injury [33]. Moreover, not only is the injury exacerbated, but the ability to protectively precondition the heart is also abolished in the absence of caveolins [108,109]. With Cav-3 overexpression, the heart is protected from ischaemia-reperfusion injury [30]. Furthermore, introduction of a Cav-1 peptide, consisting of solely of its scaffolding domain, reduced cardiac dysfunction following a period of ischaemia-reperfusion[110]. Moreover, during simulated ischaemia-reperfusion, volatile anesthetic preconditioning increased the number of caveolae in the cardiomyocyte cell membrane [108].

Caveolae interact with components of the RISK and SAFE pathways. The scaffolding domain of caveolin interacts with and modulates a variety of signaling moieties. First off, the scaffolding domain interacts with components of the RISK pathway [111,112]. The protein AKT localizes to the cellular membrane to be activated [112]. The Cav-1 scaffolding domain interacts and negatively regulates two phosphatases that are responsible for the deactivation of AKT[30,113]. Thus, by inhibiting the inhibitor, Cav-1 promotes signaling of the RISK

pathway[113]. As for the SAFE pathway — STAT3 localizes to the plasma membrane and interacts with Cav-1 [105].

1.3.12 Endothelin receptor signaling

The endothelin receptors — specifically the isoforms ETAR and ETAB are most well known for their role in the endothelium in mediating vasoconstriction/ vasoreleaxation [114]. ETAR is located upstream of the signaling cascade of both the RISK and SAFE pathways[114–117]. Activation of ETAR activates the mitogen-activated kinase (MAPK) kinase system, including ERK1/2, which decreases apoptosis [118]. Additionally, the PI3K/AKT system is activated as evidenced by increasing phosphorylation of PI3K, AKT, and other components of the RISK pathway through ETAR [114–116]. Moreover, a ligand of ETAR, endothelin 1 (ET-1) inhibits apoptosis; this protection is abrogated in the presence of a selective ETAR inhibitor, but not a selective ETBR inhibitor [119]. Endothelin receptors also activate the SAFE pathway — by causing induction of activation of JAK2 and STAT3 [117]. Thus the endothelin receptor may be involved in propofol-mediated signaling. (Refer to **Illustration 1**).

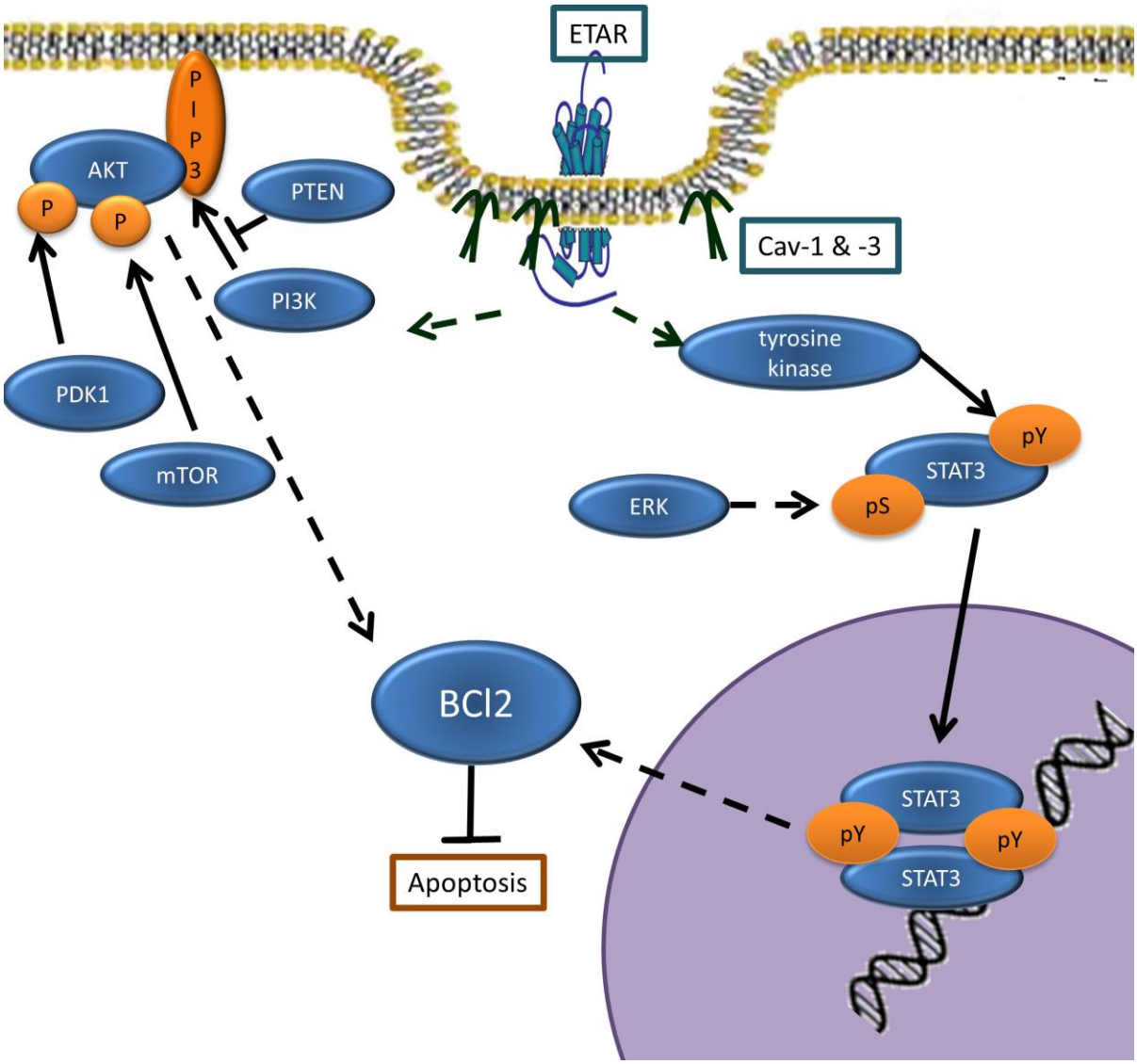

Illustration 1. Activation of SAFE and RISK pathway members leading to cellular protection.
ETAR can be found in caveolae, and caveolins form high molecular weight homo- and hetero- oligomers. **SAFE pathway**: Receptor activation leads to tyrosine kinase activation, which in turn phosphorylates STAT3 Y705. Other ERK dependent and independent pathways lead to pSTAT3 S727 phosphorylation. pSTAT3 Y705 dimerizes, translocates to the nucleus and acts as a transcription factor. **RISK pathway**: AKT associates with PIP3 in the membrane and is phosphorylated by PDK1 and mTOR (or DNA-PK). Anti-apoptotic components lie downstream. Solid arrows represent direct interactions, and dotted lines indirect interactions.

Chapter 2: Rationale, hypothesis and specific aims

2.1 Rationale

Ischaemia-reperfusion injury remains a problem during cardiac surgery. Particularly for high risk patients (e.g. patients with diabetes), it poses a threat of further morbidity and in extreme cases, mortality [60]. Fortunately, use of propofol is associated with diminished injury and better outcomes [67,73,83,120].

Propofol has a high affinity for the plasma membrane, in part due to its hydrophobic properties [48]. Potential membrane targets of propofol are caveolae (small, cholesterol, and sphingomyelin-rich plasma membrane concavities), which are abundant in signaling complexes such as endothelin receptors, and are dependent on caveolin for proper structure and function, and the endothelin receptors themselves. Aside from housing endothelin receptors, caveolae are also important components of functional protective signaling [33]. Previous in vitro studies from the Ansley laboratory demonstrate propofol-mediated prosurvival signal activation (e.g. STAT3 and AKT phosphorylation) [77,79,97]. STAT3 and AKT are components of the protective SAFE and RISK pathways, respectively [95]. ETAR, aside from interacting with Cav-1, activates both components of the RISK, and SAFE pathway (i.e. both propofol treatment and ETAR activation result in similar signal protein cellular expression levels in the cell) [114–117]. See **Illustration 1** for visualization of ETAR and caveolae's potential location in signaling events

Although certain downstream cytoplasmic components have been identified and investigated as part of the propofol-induced signaling cascade, the initial points of signal activation, with implicated membrane involvement have yet to be elucidated. These points could make lucrative targets for alleviating ischaemia-reperfusion injury via other therapeutic approaches.

2.2 Hypothesis

Propofol-mediated signaling is dependent on ETAR and caveolin.

2.3 Aims

1. To explore components of propofol signal activation
    I. To determine if ETAR is necessary for propofol-mediated signaling to occur
    II. To determine if caveolae are necessary for propofol-mediated signaling to occur
2. To explore propofol signal propagation as it relates to RISK pathway — AKT and ETAR
    I. To determine if propofol alters the interaction between ETAR and RISK pathway components (namely AKT)
    II. To determine if propofol alters ETAR cellular localization

III. To determine if there is a correlation between ETAR and Cav-1 cellular changes

3. To explore propofol signal propagation as it relates to caveolae

I. To determine if propofol changes cellular levels/ localization of Cav-1

II. To determine if propofol changes cellular levels/ localization of Cav-3

Chapter 3: Methods

3.1 Cell culture

The *Rattus norvegicus* heart myoblast cell line (H9c2) was obtained from the American Tissue Culture Collection (CRL-1446). Cells were grown in Dulbecco's modified Eagle's medium (DMEM) containing 4.5g/L D-glucose, L-glutamine, and 110mg/L D-glucose. The DMEM is supplanted with 10% fetal bovine serum (FBS), and 1% penicillin-streptomycin (5000U/mL) antibiotics. Cells were incubated at 37°C with 5% CO_2. The media was changed every three days. Upon reaching confluence the cells were passaged (briefly: washed with Dulbecco's phosphate buffered saline (DPBS), detached with trypsin, centrifuged, pellet resuspended, and re-plated). Cell passages 2 – 5 were used for experiments.

Prior to any treatment cells were exposed to starvation media which consisted of DMEM supplanted with 0.5% FBS, and 1% penicillin-streptomycin for 48 hours.

3.2 Reagents

Cell culture reagents, including DMEM, streptomycin/ penicillin, trypsin, FBS, and DPBS were purchased from Life Technologies, Thermo Fischer Scientific. Cell lysis buffer was purchased from Cell Signaling.

The primary antibodies mouse anti-pSTAT3 Y705, rabbit anti-pSTAT3 S727 were purchased from Cell Signaling Technology. Rabbit anti-Cav-1, rabbit anti-Cav-3, mouse-anti-ETAR, rabbit-anti-AKT were from Santa Cruz Biotechnology. Mouse anti-β actin was from Applied Biological Materials (ABM). The secondary, horseradish peroxidase conjugated antibodies — goat anti-mouse and goat anti-rabbit were also from ABM. Secondary Fluorescein (FITC) and Cyanine (Cy)3 conjugated anti-mouse and anti-rabbit antibodies were from Jackson ImmunoResearch Laboratories, Inc.

The ETAR specific inhibitor, PD156707 was from Sigma Aldrich Corporation, as was dimethyl sulfoxide (DMSO), propofol, methyl-β-cyclodextrin, protease inhibitor cocktail (p8340), phenylmethylsulfonylfluoride (PMSF), Bovine Serum Albumin (BSA), and poly-D-lysine.

Serological pipettes, cell culture flasks, centrifuge tubes, Eppendorf tubes, pipet tips, and other disposables were from VWR International.

Ultracentrifuge tubes were from Beckman Coulter. 2-(N-Morpholino)ethanesulfonic acid (MES) sodium salt was from Sigma Aldrich Corporation. Sodium carbonate and sucrose were from Bio Basic Inc.

Western blot reagents were from Bio-Rad Laboratories Inc. — 4x Laemmli Buffer, Stacking Gel Buffer (0.5M Tris-HCl), Resolving Gel Buffer (1.5M Tris-HCl), 30% acrylamide 29:1, and Bio-Rad Protein Assay Dye Reagent Concentrate.10% w/v sodium dodecyl sulphate

(SDS) was from Bio Basic Inc. SuperSignal West Femto Maximum Sensitivity Substrate was from Life Technologies, Thermo Fisher Scientific. Non-fat dry milk was from Santa Cruz Biotechnology.

Protein G plus Protein A Agarose Suspension was from Calbiochem, EMD Millipore. Fluoromount-G was from Southern Biochem. Coverslips and glass microscope slides were from Thermo Fisher Scientific. The nuclear staining dye, bisbenzimide H 33258 fluorochrome (Hoechst 33258) was from Calbiochem.

3.3 Propofol treatment

For all treatment conditions, pure propofol was diluted in DMSO to a concentration 50mM. It was further diluted in starvation media to final working concentrations of either 25μM or 50μM as called for by the experiment.

The control conditions were treated with an equivalent amount of vehicle (DMSO). (Treating control with vehicle ensured that any biological effect seen was not due to DMSO).
The H9c2 cells were then incubated with propofol for 30 minutes. Subsequently, cells were washed three times with ice cold DPBS. Cells were lysed by incubating with Cell Signaling lysis buffer (20mM Tris-HCl (pH 7.5), 150mM NaCl, 1mM Na_2EDTA, 1% Triton, 2.5mM sodium pyrophosphate, 1mM β-glycerophosphate, 1mM Na_2VO_4, 1μg/mL leupeptin) (with 1mM PMSF added just prior to use) on ice for 5 minutes. Cells were scratched, lysates collected, and finally sonicated for 10 seconds at 60% capacity.

Cell lysates were centrifuged at 12000RPM for 10 minutes to pellet out unlysed cells and cellular debris.

3.4 Protein quantification — Bradford protein assay

Protein quantification was done using a Bradford assay. The Bradford assay takes advantage of an absorbance shift at 595 nm when the dye reagent binds to protein (in this study we used Bio-Rad Protein Assay Dye Reagent). The dye reagent is incubated with protein sample for ten minutes prior to reading the 595nm absorbance value with a spectrophotometer. To determine protein concentration levels, first, a calibration curve (absorbance vs. concentration) is created from a set of BSA standard solutions (with concentrations evenly covering concentrations from 0 to 25μg/mL). Subsequently, the calibration curve can be used to determine sample protein concentrations.

3.5 Western blot

Samples were mixed with 4x Laemmli Buffer with 5% β-mercaptoethanol and boiled for ten minutes at 100ºC.

Samples were separated using SDS polyacrylamide gel electrophoresis (SDS-PAGE). Based on the Bradford assay, 25μg of protein sample were loaded per well. Depending on the molecular weight of the target protein (and in order to attain optimal resolution), 10 or 12% acrylamide gels were run. Applying a voltage across the gel, the proteins separated as they

migrated towards the anode. Upon completion of the gel run, the gel was transferred to a nitrocellulose membrane overnight at 4^{o}C.The membrane was then blocked in 5% skim milk, washed thoroughly in TBS-Tween, and incubated 1:1000 with primary antibodies as indicated in 5% BSA overnight at 4^{o}C (except for the anti-β-actin antibody which had a dilution of 1:10000). Subsequently, the membrane was washed in TBS-Tween, and incubated 1:10000 for 2 hours with the appropriate (either anti-mouse or anti-rabbit) HRP-conjugated antibody. The membrane was subsequently washed and developed using West Femto Maximum Sensitivity Substrate. Membrane imaging was done using FluorChem (ProteinSimple), and semi-quantitative densitometry analysis using ImageJ (v.149) software (National Institute of Health). The densitometry was expressed relative to control and standardized to β-actin.

3.6 Co-immunoprecipitation

H9c2 cells were starved at 80% confluence for 48 hours, and then treated with either 0μM (control), 25μM, or 50μM of propofol for a 30 minute period at 37°C. All conditions had a final DMSO concentration of 0.1%. The cells were lysed and processed as per standard protocol.

Lysates were centrifuged at 3000RPM for 3 min in order to remove any cellular debris. The samples were then centrifuged at 10,000 RPM for 60 minutes at 4°C. The supernatant (cytosol) was removed and the pellet (membrane) was washed and resuspended in 20mM

Tris-HCl (pH 7.5) containing 1:100 protease inhibitor. The sample was centrifuged and washed a further two more times.

Protein concentrations were determined via Bradford as mentioned in section 3.4. 225µg of protein were used for the subsequent Co-IP. Samples were incubated with 2µg of primary antibody overnight at 4ºC. Subsequently samples were incubated with 25µL of Protein G plus Protein A Agarose beads, at room temperature, for 2 hours. The samples were then centrifuged at 5000RPM for 5 min and the supernatant discarded. The beads and sample were further washed 3 times with DPBS. Finally Laemmli buffer (with 5% β-mercaptoethanol) was added to the sample, and subsequently boiled for 10 minutes. (This step served to dissociate the protein from the beads). The samples were briefly spun again, and the supernatant was loaded and a Western blot run as described in section 3.5.

3.7 Discontinuous sucrose density gradient

Cells were grown and treated as per the standard procedure outlined above, except for the following changes. After cells were washed 3X with cold DPBS following treatment, they were lysed via incubation with 500mM Na_2CO_3 (pH 11, containing 2x protease inhibitors) at 4^oC for 10 minutes. The samples were sonicated at 60% for 2x10s.

A 5 – 42.5% gradient was created in Beckman Coulter centrifuge tubes, with sample at the bottom. The cell lysate (2mL) was mixed with 2mL of 85% sucrose (in MES buffered saline (MBS) buffer (25mM MES, 0.15M NaCl). After letting the sucrose solution set for 2 hours it

was then overlaid with 6mL 30% sucrose (MBS buffer, 250mM Na_2CO_3). Finally, the sucrose gradient was overlaid with 2mL of 5% sucrose (MBS buffer, 250mM Na_2CO_3). The samples were then centrifuged for 20 hours at 24000RPM in a SW21 rotor in an ultracentrifuge (Beckman Coulter, Inc.). The fractions were then removed 1mL at a time — the top of the centrifuge tube became fraction "1", and the bottom will have been fraction "12."

An equal amount of each fraction was loaded and a Western blot was run as described earlier. The density of each band was quantified, and was expressed as a proportion of the total density of the entire plot.

3.8 Immunocytochemistry

Glass cover slips were prepared by washing in concentrated HCl to aid poly-D-lysine adherence. Coverslips were placed in a 24 well plate and coated with poly-D-lysine. After washing the coverslips (twice with water, once with DPBS), cells were plated, and grown under standard protocol culture conditions, except for the final confluence (which was approximately 70%). Cells were treated with propofol as per protocol. Following the 30 minute propofol treatment period, cells were immediately fixed with 4% paraformaldehyde for 20 minutes at room temperature. They were then washed with DPBS thoroughly. Then, cells that were to be in the completely permeabilized condition were treated with 0.2% Triton-X-100 detergent for 15 minutes at room temperature. The Triton was then removed, and the cells washed again with DPBS. All the cells were then blocked in 5% Normal Goat

Serum (NGS) for one hour. The samples were then incubated overnight in 1:400 primary antibody in 5% NGS at 4ºC. The samples were then washed with DPBS and incubated with fluorescent secondary antibodies — Cy3 (red)-anti-mouse or anti-rabbit and/ or FITC (green)-anti-mouse or anti-rabbit at a dilution of 1:500 in DPBS for 90 minutes. Three experimental controls were used to eliminate the possibility of autofluorescence, or background non-specific fluorescence of the antibodies: 1) no antibodies; 2) primary antibodies alone; 3) secondary antibodies alone. Nuclei were stained with Hoechst. Coverslips were mounted on glass microscope slides with Fluoromount-G.

Fluorescence was visualized using an Olympus fluorescence microscope, the 40X or 63X oil based objective (Olympus Corporation). Q Capture 6.0 pro was used to capture the fluorescent images. The intensity of the fluorescence (corresponding to protein level) was determined using ImageJ (v.149) based on the method as reported previously by [121].

3.9 Statistical analysis

Statistics were done using GraphPad Prism 5.03 (GraphPad Software). Results were analyzed using a one-way ANOVA with a Tukey's HSD post hoc test. Grubb's test for outliers was used, and the outlier removed. The level of significance was set to $p < 0.05$. Results are presented as mean $\pm$ standard deviation (SD).

Chapter 4: Results

4.1 Propofol signal activation

4.1.1 ETAR inhibition decreases phosphorylated STAT3 Y705

The Ansley laboratory has previously demonstrated that propofol increases levels of pSTAT3 Y705 and pSTAT3 S727 in H9c2 cardiomyoblasts [97]. Likewise, ETAR activation also has the ability to induce STAT3 phosphorylation [117]. Accordingly, ETAR was initially selected as a good potential candidate for signal activation in our experiments.

In order to examine the dependence of propofol signaling on ETAR, H9c2 cardiomyoblasts were pretreated with the selective ETAR inhibitor PD156707 (5, 10, or 15μM) in the presence or absence of propofol (50μM). Levels of phosphorylated STAT3 (both S727 and Y705) were determined using Western blot.

Compared to control, PD156707 decreased pSTAT Y705 levels (**Figure 1**). The decrease was significant at PD156707 concentrations of 10 and 15μM. In response to propofol, pSTAT Y705 levels increased, albeit non-significantly. Inhibition of ETAR in propofol-treated conditions significantly decreased pSTAT3 Y705 levels in relation to propofol treatment alone.

Compared to control, pSTAT3 S727 tended to increase in response to PD156707 (5, 10, or 15μM) or 50μM (**Figure 2**). However, the observed increase did not achieve statistical significance in our model. Moreover, PD156707 application did not decrease levels of pSTAT3 S727. The results suggest that propofol-mediated pSTAT3 Y705, and not S727, is ETAR dependent. Thus, for further studies involving propofol signaling, only pSTAT3 Y705 levels were determined.

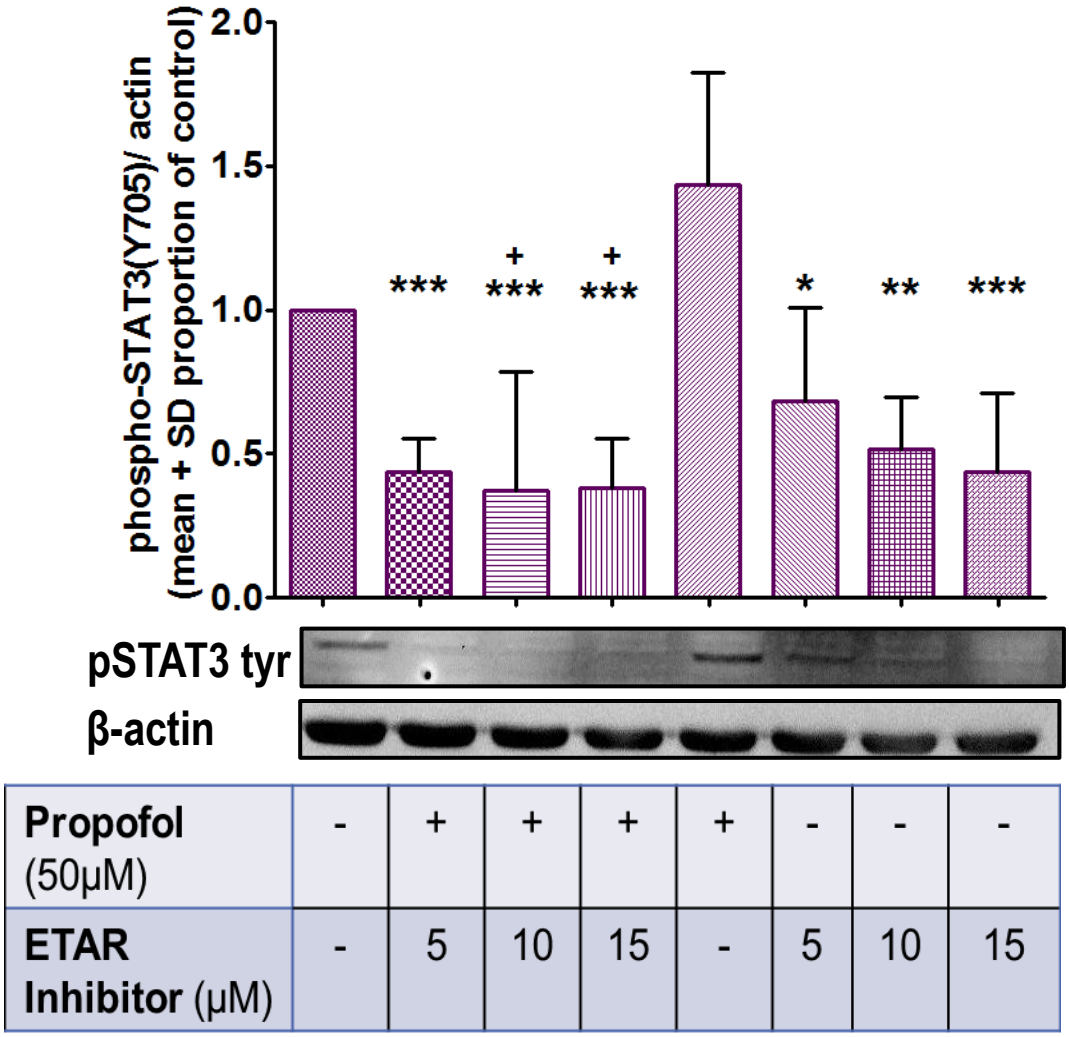

Figure 1. Propofol-mediated STAT3 Y705 phosphorylation is ETAR dependent. H9c2 cells were treated with the selective ETAR inhibitor PD156707 (5, 10 or 15μM) for 30 minutes prior to the addition of 50μM of propofol for 30 minutes. pSTAT3 Y705 levels were determined via Western blot. *p<0.05 relative to propofol 50μM, **p<0.01 relative to propofol 50μM, ***p<0.001 relative to propofol 50μM, +p<0.05 relative to control n = 4 – 5. (Outliers were removed: in the second group a value of 1.71, and in the fifth group a value of 5.33).

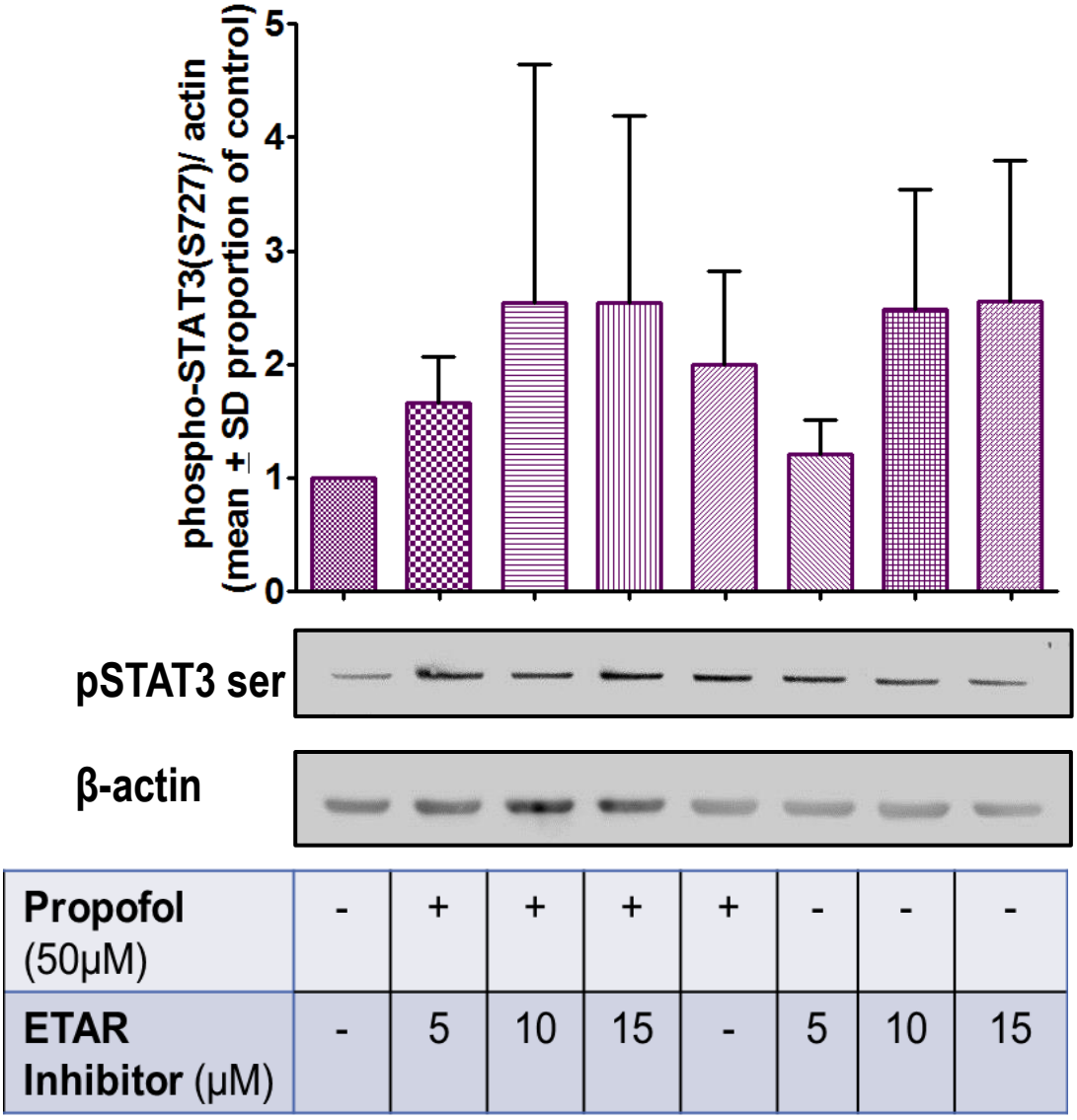

Figure 2. Propofol-mediated STAT3 S727 phosphorylation is ETAR independent. H9c2 cells were treated with the selective ETA receptor inhibitor PD156707 (5, 10 or 15μM) for 30 minutes prior to the addition of 50μM of propofol for 30 minutes. pSTAT3 S727 levels were determined via Western blot. n = 3 – 4. (Outlier was removed: a value of 5.31 in the second group).

4.1.2 Lipid raft disruption does not decrease phosphorylated STAT3 Y705.

ETAR receptors are enriched in caveolae, a subtype of lipid raft [6]. The role of caveolae in propofol-mediated protection, especially as it relates to signal activation has not previously been explored.

Lipid rafts can be disrupted by removing cholesterol. Typically, cholesterol depletion interrupts cellular signaling.

In the present study lipid rafts were disrupted by cholesterol depletion with methyl-β-cyclodextrin, and propofol signaling evaluated (**Figure 3**). Phosphorylated STAT3 Y705 levels increased in H9c2 cardiomyoblasts treated with both propofol (50μM) and methyl-β-cyclodextrin.

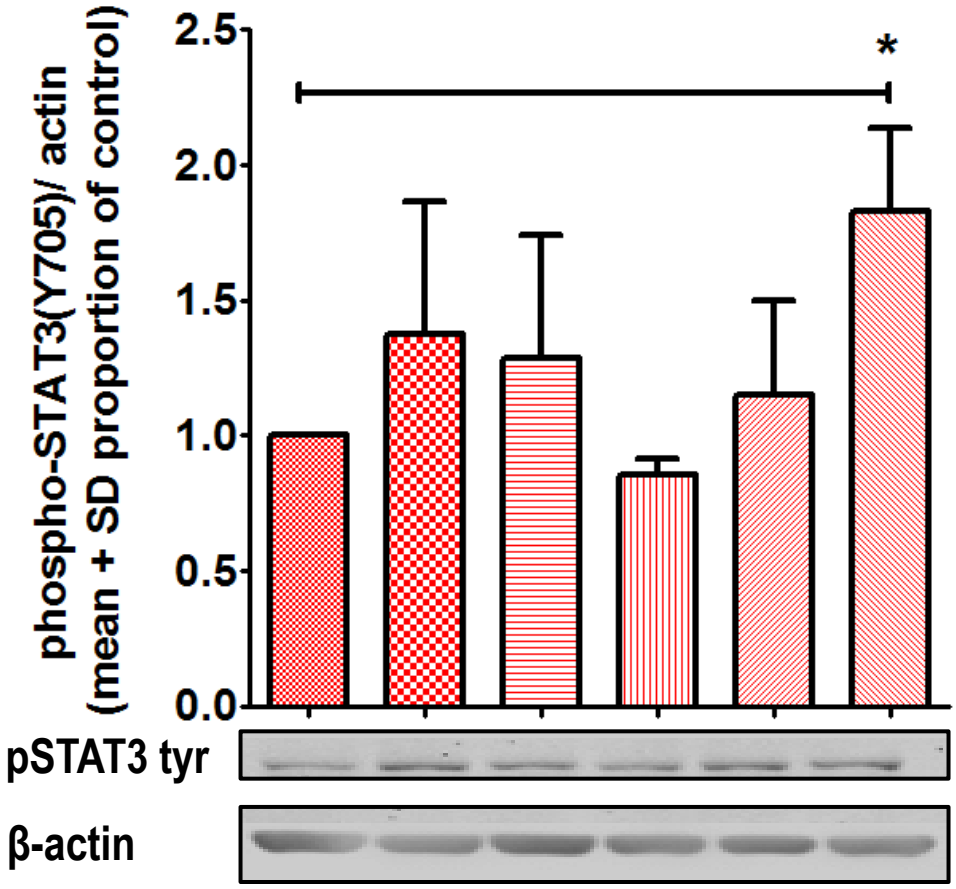

Propofol (μM)	-	25	50	-	25	50
mβCD (5mM)	-	-	-	+	+	+

Figure 3. Propofol-mediated pSTAT3 Y705 signaling occurs despite lipid raft disruption.

H9c2 cells were pretreated with 5mM methyl-β-cyclodextrin for 30 minutes, and subsequently treated with 25μM or 50μM of propofol as per standard protocol. pSTAT3 Y705 expression was measured using Western blot as a function of propofol signaling. *$p<0.05$, n= 2 – 4. An outlier with a value of 2.78 was removed from the fourth group.

4.2 Propofol signal trafficking

Beyond propofol signal activation at the cellular membrane, cellular signal progression and propagation is of additional interest, and not fully explored. Protein effector interaction and cellular localization changes we subsequently studied.

4.2.1 RISK pathway involvement: AKT and ETAR

Previously our laboratory has shown that propofol increases expression/ activation of components of the RISK pathway, including phosphorylation of AKT [97].

4.2.1.1 AKT interacts with ETAR

ETAR interacts with AKT [122]. We investigated the AKT-ETAR interaction using Co-IP in the context of propofol treatment. An interaction between AKT and ETAR (**Figure 4A, B)** was suggested by AKT's ability to Co-IP with ETAR. This result was validated by a reverse Co-IP in which an AKT primary antibody was used for immunoprecipitation and ETAR protein was detected. ETAR Co-IPs with AKT (and vice versa) under control conditions. Furthermore, and more importantly, ETAR's ability to Co-IP AKT is retained when cells are treated with propofol.

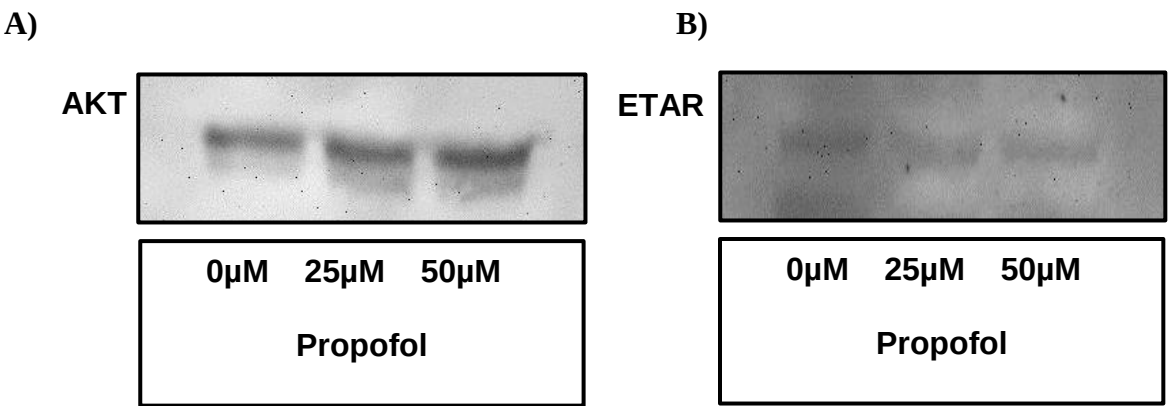

Figure 4. Co-immunoprecipitation of AKT and ETAR: AKT immunoprecipitates with ETAR and ETAR immunoprecipitates with AKT.
H9c2 cells were treated with the indicated amounts of propofol for 30 minutes. Samples were then differentially centrifuged and the cellular membrane and nuclear fractions condensed and used for immunoprecipitation **A)** Samples were immunoprecipitated with ETAR primary antibody, and subsequently were probed for the presence of AKT **B)** The reverse Co-IP, samples were immunoprecipitated with AKT antibody and probed for ETAR.

4.2.1.2 Propofol does not alter AKT cellular distribution.

H9c2 cells were either partially permeabilized (as a result of the fixation with 4% paraformaldehyde), or were completely permeabilized (addition of 0.2% Triton-X-100 after paraformaldehyde fixation). Partial permeabilization allows visualization of proteins close to the membrane. Complete permeabilization exposes the entire cytoplasm to antibodies, and consequently allows intracellular visualization via immunofluorescence. Cellular distribution of AKT in H9c2 cells (as visualized by immunofluorescence) did not change with propofol treatment — neither with partial permeabilization (**Figure 5)**, nor with complete permeabilization (**Figure 6)**. Intracellular AKT localized to the nuclear region under completely permeabilized conditions, regardless of propofol concentration.

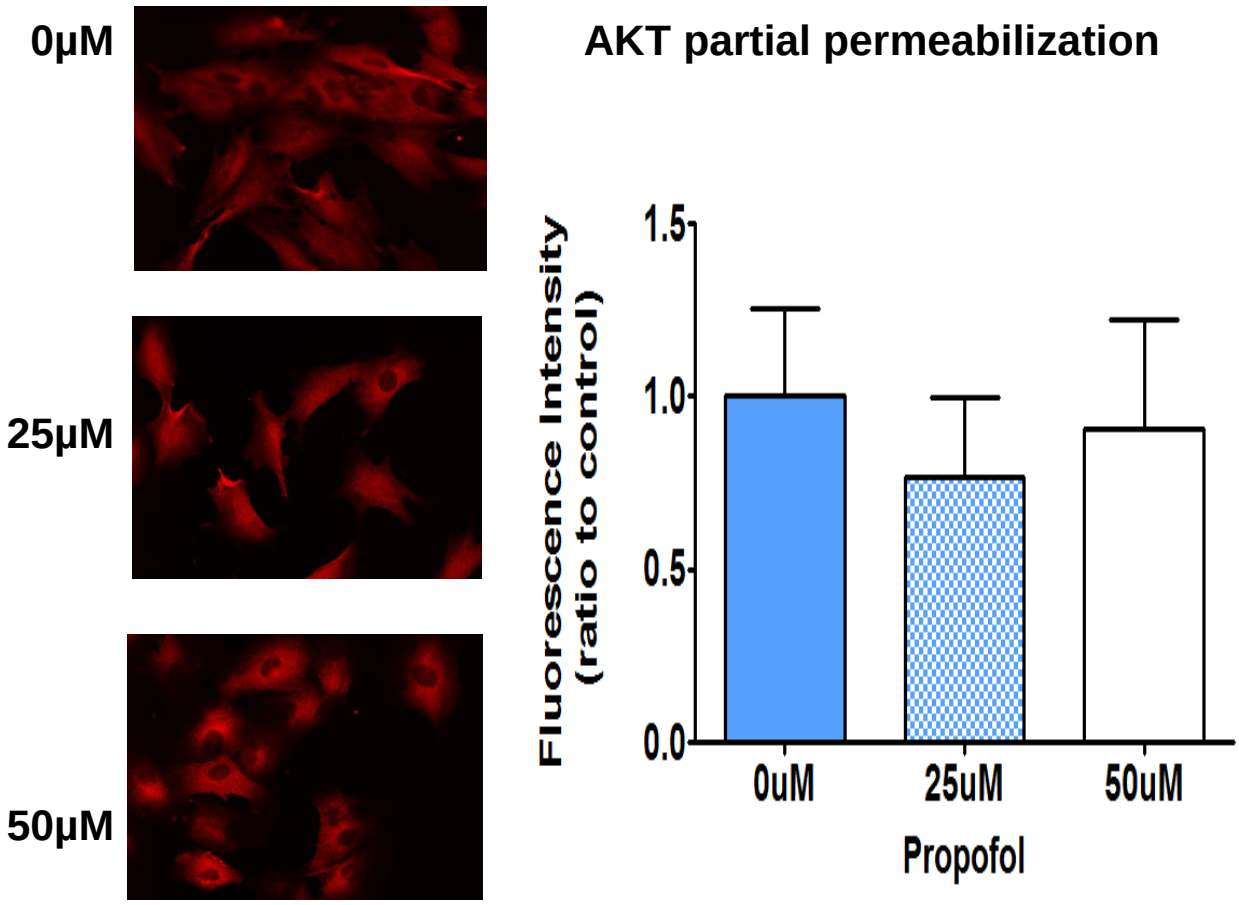

Figure 5. AKT distribution unchanged with propofol treatment.

H9c2 cells were treated for 30 minutes with 0μM, 25μM, or 50μM of propofol and then partially permeabilized. They were immunofluorescently stained for AKT (red). The experiment was repeated twice and an image from a representative coverslip is shown. A similar fluorescence intensity trend was seen across all repeats. The mean ± SD of the images taken from the representative coverslip is shown. Fluorescence intensity of AKT was quantified using ImageJ. n = 3 – 5

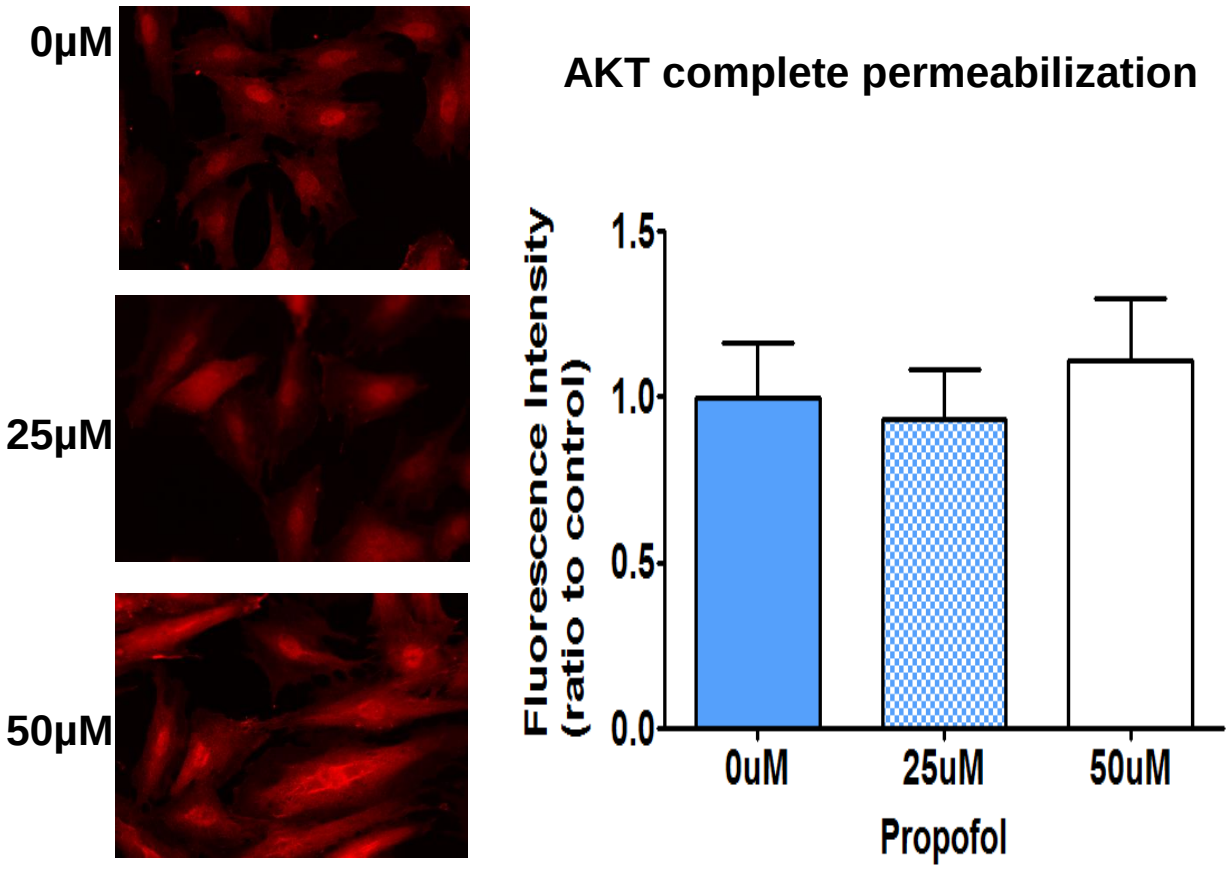

Figure 6. AKT distribution unchanged with propofol treatment.

H9c2 cells were treated for 30 minutes with 0μM, 25μM, or 50μM of propofol and then completely permeabilized. They were immunofluorescently stained for AKT (red). The experiment was repeated twice and an image from a representative coverslip is shown. A similar fluorescence intensity trend was seen across all repeats. The mean ± SD of the images taken from the representative coverslip is shown. Fluorescence intensity of AKT was quantified using ImageJ. n = 5.

4.2.2 Propofol increases intracellular levels of ETAR

Next, propofol's effect on cellular distribution of ETAR was examined via immunocytochemistry. Under partial permeabilization conditions a difference in levels of ETAR expression was not detected (**Figure 7A, B**). Alternatively, when H9c2 cardiomyoblasts were completely permeabilized with detergent, allowing the antibodies to

fully permeate intracellularly, propofol (50μM) significantly increased ETAR levels (**Figure 8A, B**).

In addition, ETAR was localized to puncta, in a predominantly perinuclear locale (**Figure 8**). The cellular periphery is largely devoid of ETAR. Moreover, even though propofol increased fluorescence intensity (which corresponds to increased protein expression), propofol did not alter the spatial pattern of ETAR expression.

4.2.3 ETAR and Cav-1 peri-plasmalemmal colocalization

ETAR colocalizes with Cav-1 [123]. Extensive colocalization of ETAR and Cav-1 occurred close to the plasma membrane, as represented by the yellow overlap of red (ETAR) and green (Cav-1) pixels in the partially permeabilized condition (**Figure 7A** merged). However, Cav-1 and ETAR distributions intracellularly minimally overlapped (**Figure 8A** merged). Cav-1 was distributed throughout the cell, but particularly at the periphery of the cell. In contrast, ETAR was internally distributed in puncta (see 4.2.2).

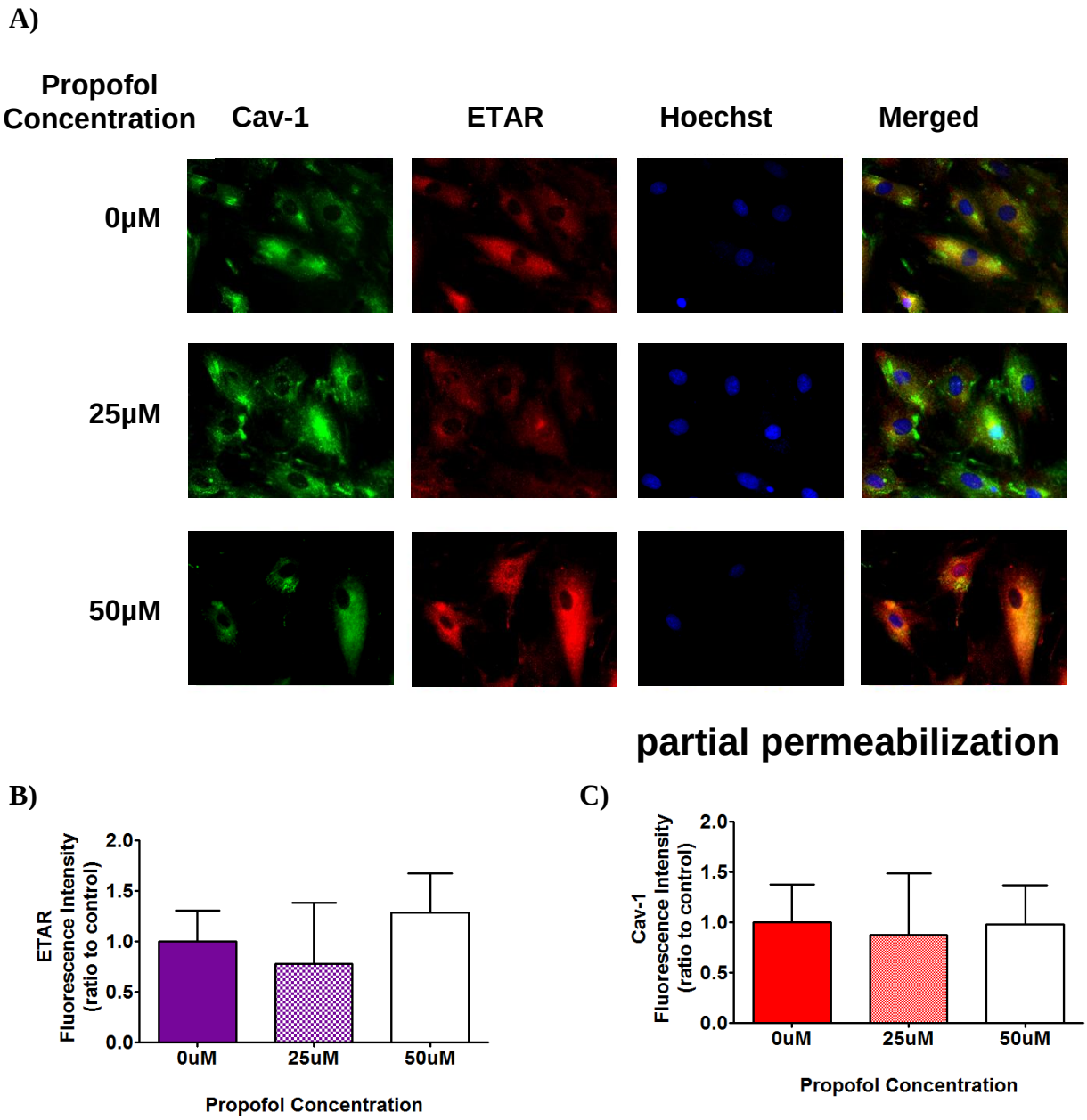

Figure 7. Propofol-mediated cellular distribution of ETAR and Cav-1: Unchanged intensity levels.

A) H9c2 cells were treated for 30 minutes with 0μM, 25μM, or 50μM of propofol and then partially permeabilized. They were immunofluorescently stained for ETAR (red), Cav-1 (green), nuclei (Hoechst; blue). The merged images are presented in the rightmost column. The experiment was repeated 3 times and an image from a representative coverslip is shown. A similar fluorescence intensity trend was seen across all three repeats. The mean $\pm$ SD of the images taken from the representative coverslip is shown (**B, C**). **B)** Fluorescence intensity of ETAR was quantified using ImageJ; n = 5 – 7 **C)** Fluorescence intensity of Cav-1 quantified using ImageJ; n = 5 – 7

A)

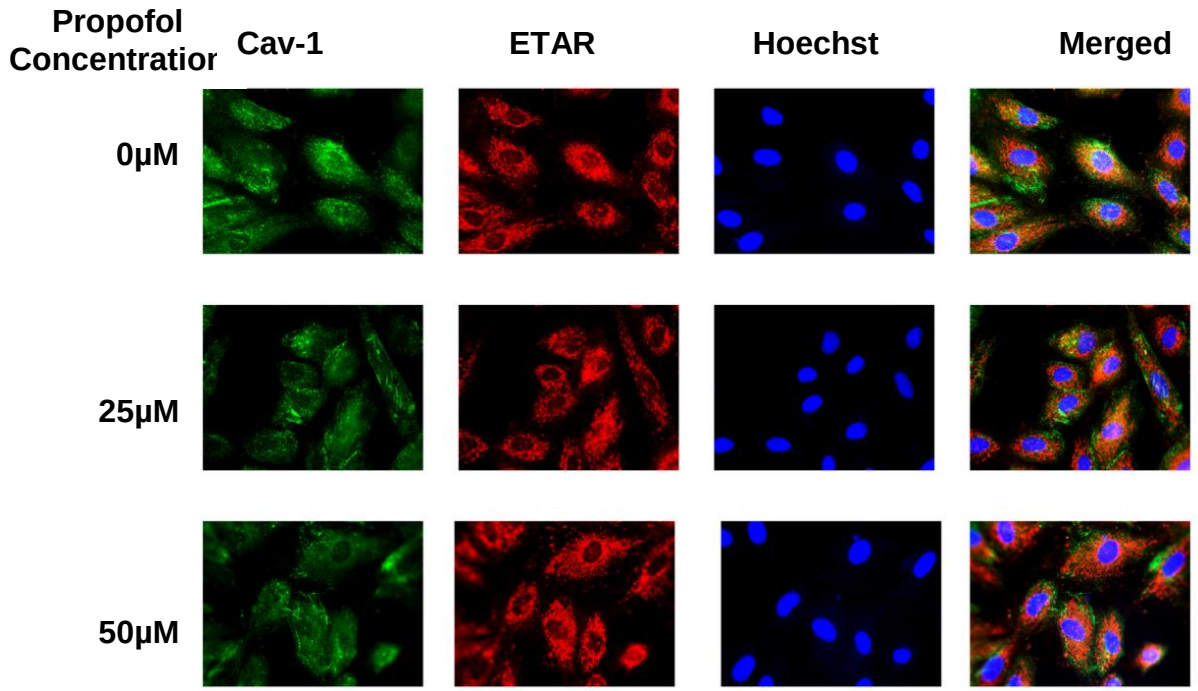

B)

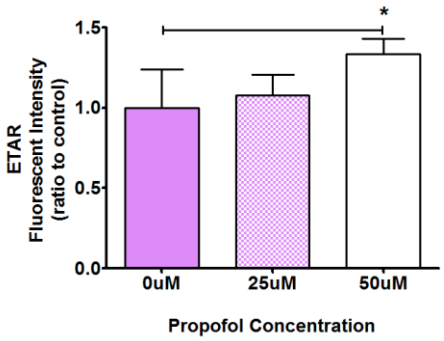

C) **complete permeabilization**

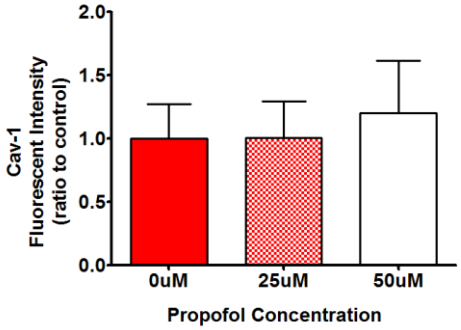

Figure 8. Propofol-mediated cellular distribution of ETAR and Cav-1: Increase in ETAR intensity levels.

A) H9c2 cells were treated for 30 minutes with 0μM, 25μM, or 50μM of propofol and then completely permeabilized (fixed with paraformaldehyde, followed by permeabilization with 0.2% Triton-X-100). They were immunofluorescently stained for ETAR (red), Cav-1 (green), nuclei (Hoechst; blue). The merged images are presented in the rightmost column. The experiment was repeated 3 times and an image from a representative coverslip is shown. A similar fluorescence intensity trend was seen across all three repeats. The mean $\pm$ SD of the images taken from the representative coverslip is shown (**B, C**). **B)** Fluorescence intensity of ETAR quantified using ImageJ; n = 4 – 6; * $p < 0.05$ **C)** Fluorescence intensity of Cav-1 quantified using ImageJ; n = 5 – 6.

4.2.4 Propofol's effect on caveolae scaffolding proteins — Cav-1 and Cav-3

In cardiomyocytes, caveolae possess both Cav-1 and Cav-3, which can interact and regulate signaling moieties, such as ETAR [6,17].

4.2.4.1 Propofol does not alter Cav-1 distribution in the cell

Immunofluorescence results suggest that propofol did not alter Cav-1 distribution in H9c2 cells — neither at the level of expression, nor at the level of spatial organization (**Figure 7A, C; Figure 8A, C**). As can be seen in **Figure 7A**, Cav-1 was diffusely spread across the cell. It was especially abundant around the edges of the cell, where it had almost no overlap with ETAR.

Results from a discontinuous sucrose fractionation (**Figure 9**) also support propofol's lack of effect on Cav-1 cellular distribution. A 5 – 42.5% discontinuous sucrose gradient was created and the samples were bottom-loaded. The samples were ultracentrifuged and organellar separation occurred to a certain extent. Light fractions, which include lipid rafts and caveolae, are located near the top of the gradient (fractions 2 – 5), and bulk cytosolic proteins are located in the lower fractions (9 – 12). β-actin was used as a control for the bulk cytosolic fractions. The percentage of total cellular Cav-1 located in the light fractions was 67.62 $\pm$ 0.62% (0μM propofol), 60.93 $\pm$ 2.26% (25μM propofol), and 64.55 $\pm$ 2.09% (50μM propofol). The cellular percentage distribution of Cav-1 amongst the 12 fractions did not significantly differ with propofol treatment (**Figure 9**).

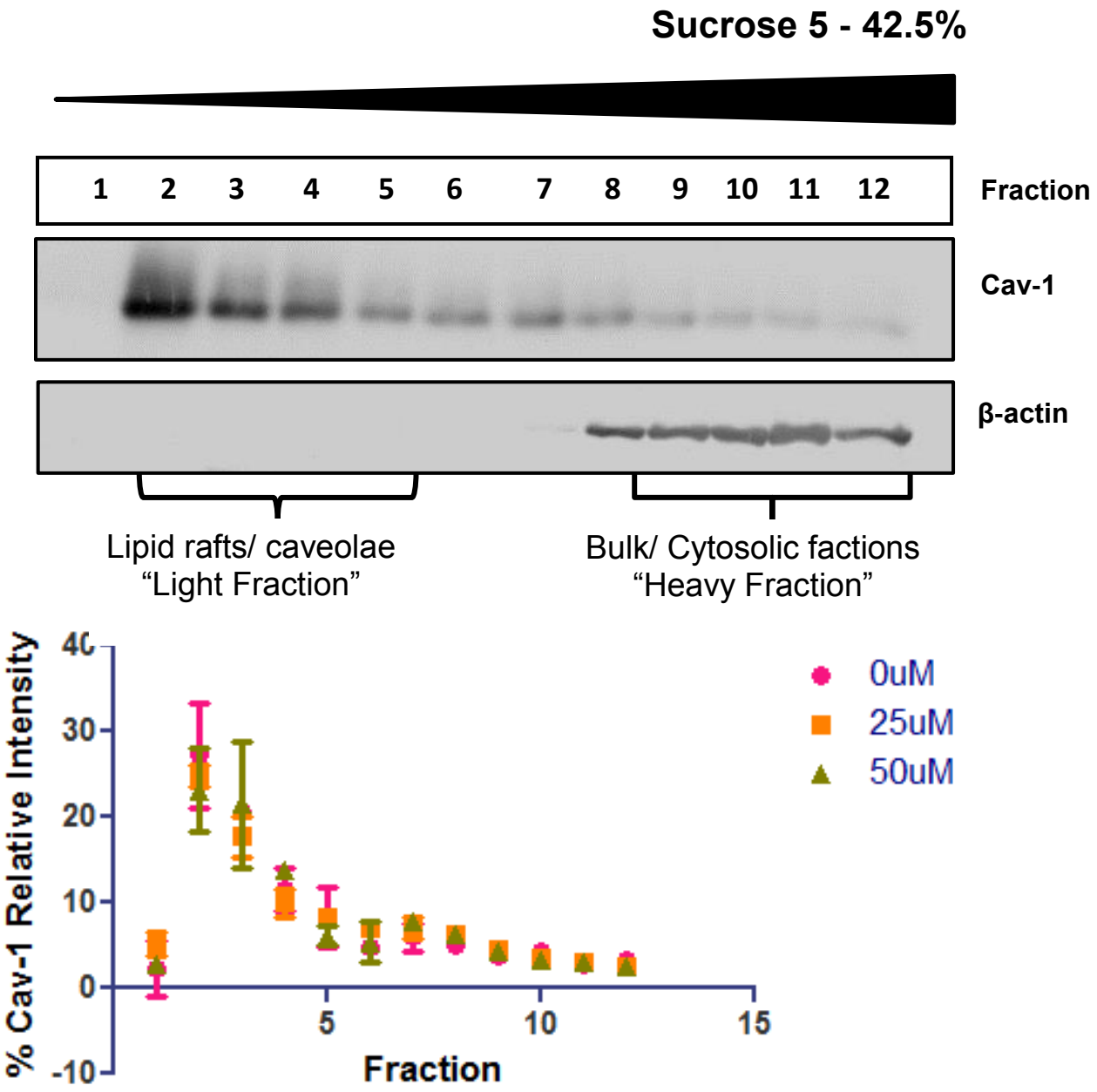

Figure 9. Cav-1 proportional raft distribution remains unchanged with propofol treatment.

H9c2 cells were treated with 0µM, 25µM, or 50µM of propofol and subsequently lysed using a detergent-free method. The samples underwent fractionation on a 5 – 42.5% (5/30/42.5%) discontinuous sucrose gradient. Twelve fractions were then collected from each sample, and a Western blot was equally loaded and run to determine the relative Cav-1 protein amount amongst the fractions. The sample blot shown above is the result of cells treated with 50µM of propofol. The amount of Cav-1 was represented as the average percentage of total Cav-1 (from fractions 1 – 12) $\pm$ SD. Pink circles represent 0µM, Orange squares represent 25µM, and green triangles represent 50µM. n = 2.

4.2.4.2 Cav-1 protein expression levels unchanged with propofol treatment

In addition to propofol's lack of effect on cellular distribution of Cav-1, propofol likewise did not affect Cav-1 whole cell lysate levels (**Figure 10**).

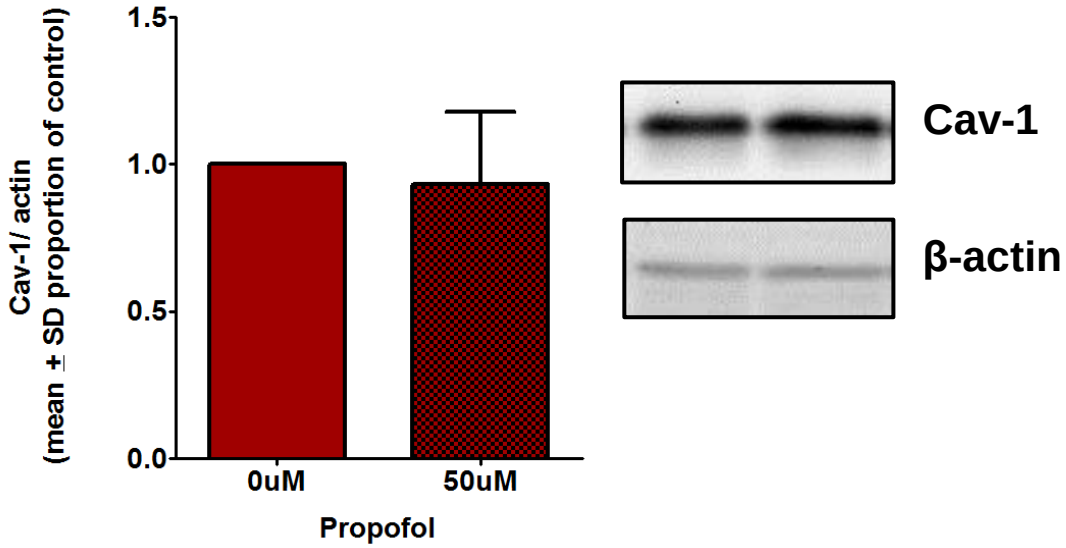

Figure 10. Whole-cell Cav-1 unchanged with propofol treatment.
H9c2 cells were treated with 50μM propofol, and whole cell levels of Cav-1 were determined via Western blot. n = 5.

4.2.4.3 Cav-3 protein expression increases in the nucleus with propofol treatment

Cav-3 protein expression increases in the nucleus with propofol treatment

Cav-3 immunofluorescence of partially permeabilized cells (**Figure 11**), and completely permeabilized cells (**Figure 12**) revealed a fluorescence intensity that did not vary significantly with varying concentrations of propofol. Furthermore, propofol did not alter Cav-3 levels in whole cell lysates (**Figure 13).** Moreover, even though Cav-3 intracellular intensity did not significantly change with propofol treatment, there was an increase of Cav-3 levels in the nucleus with 50μM of propofol treatment (**Figure 12)**.

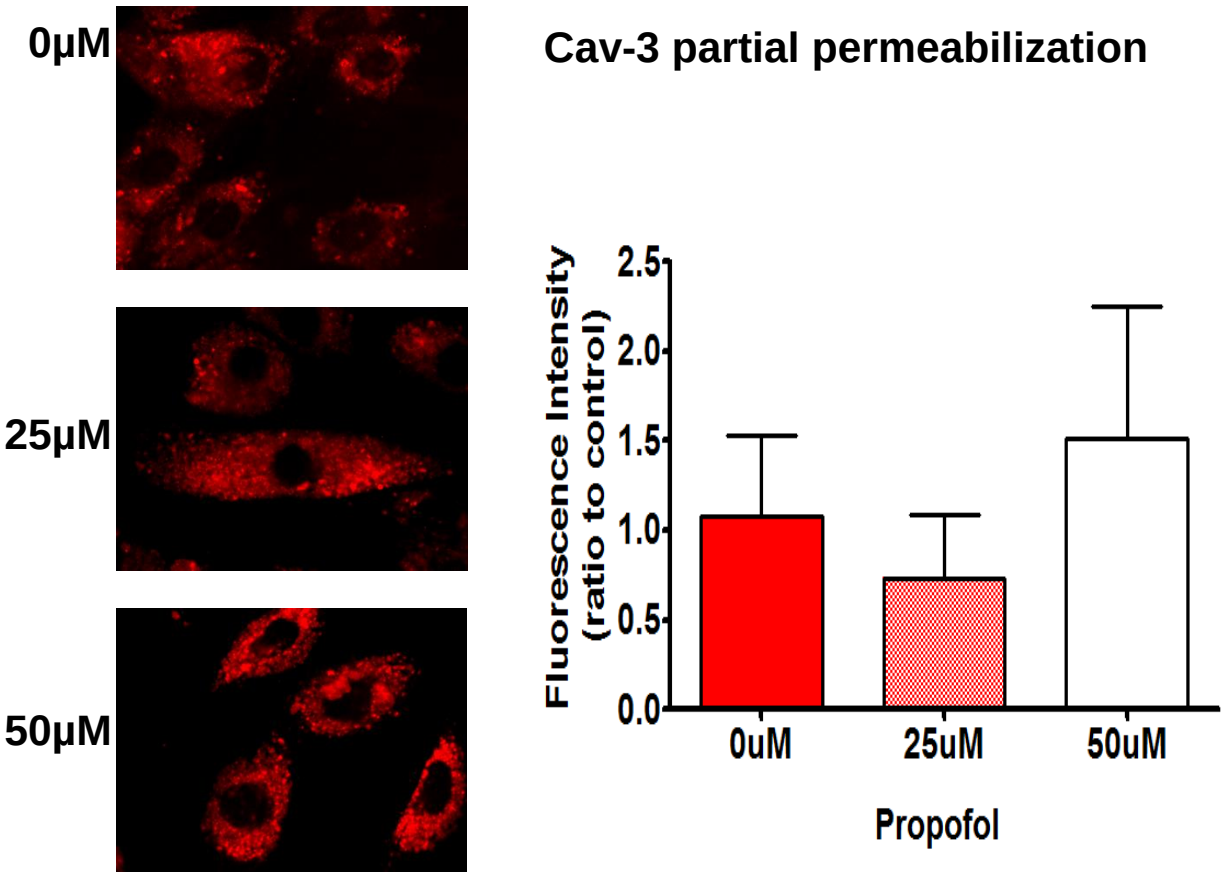

Figure 11. Cav-3 distribution unchanged with propofol treatment.
H9c2 cells were treated for 30 minutes with 0μM, 25μM, or 50μM of propofol and completely permeabilized. They were immunofluorescently stained for Cav-3 (red). The experiment was repeated three times and an image from a representative coverslip is shown. A similar fluorescence intensity trend was seen across all repeats. The mean ± SD of the images taken from the representative coverslip is shown. Fluorescence intensity of Cav-3 was quantified using ImageJ. n = 5.

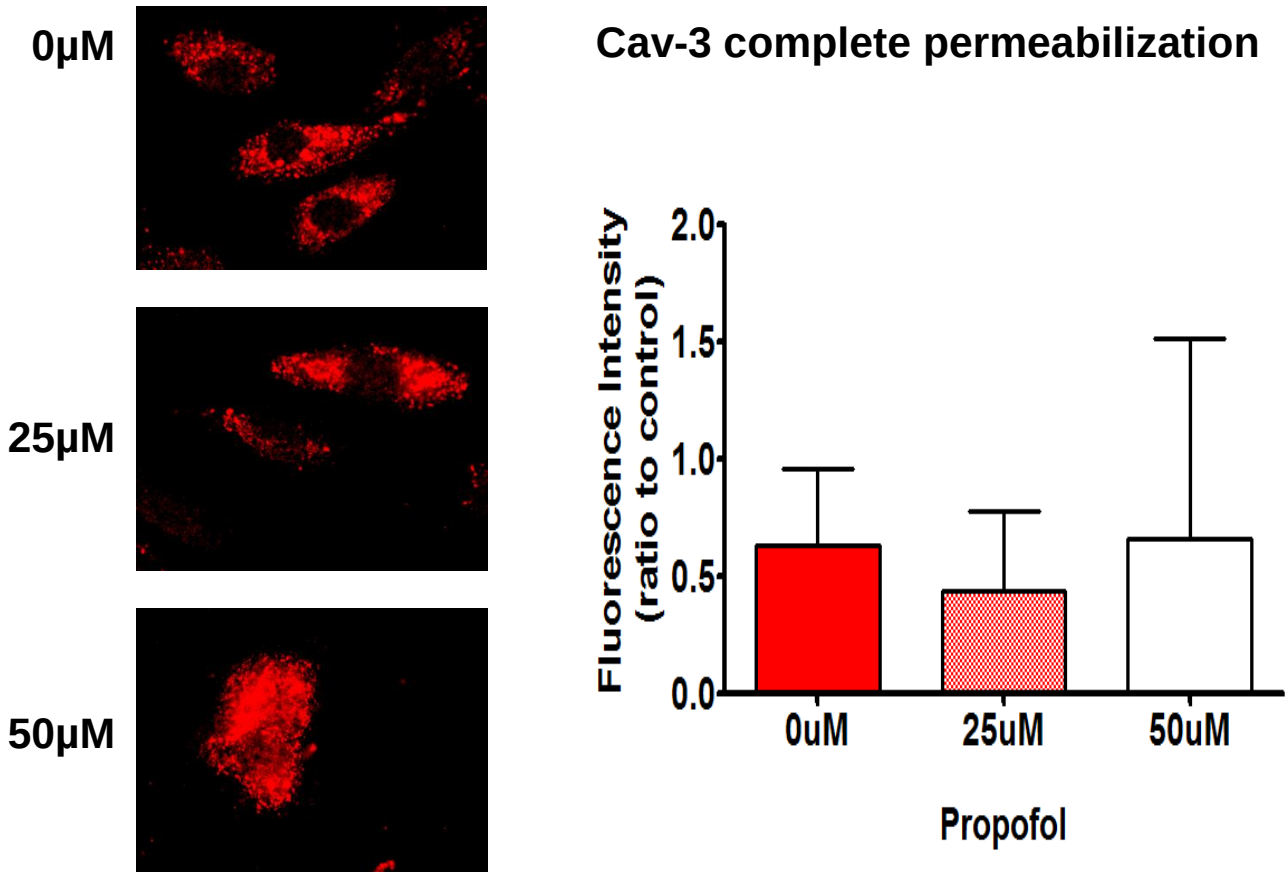

Figure 12. Cav-3 cytoplasmic intensity unchanged; Cav-3 increases in the nucleus. H9c2 cells were treated for 30 minutes with 0μM, 25μM, or 50μM of propofol and partially permeabilized. They were immunofluorescently stained for Cav-3 (red). The experiment was repeated three times and an image from a representative coverslip is shown. A similar fluorescence intensity trend was seen across all repeats. The mean $\pm$ SD of the images taken from the representative coverslip is shown. Fluorescence intensity of Cav-3 was quantified using ImageJ. n = 2 – 5.

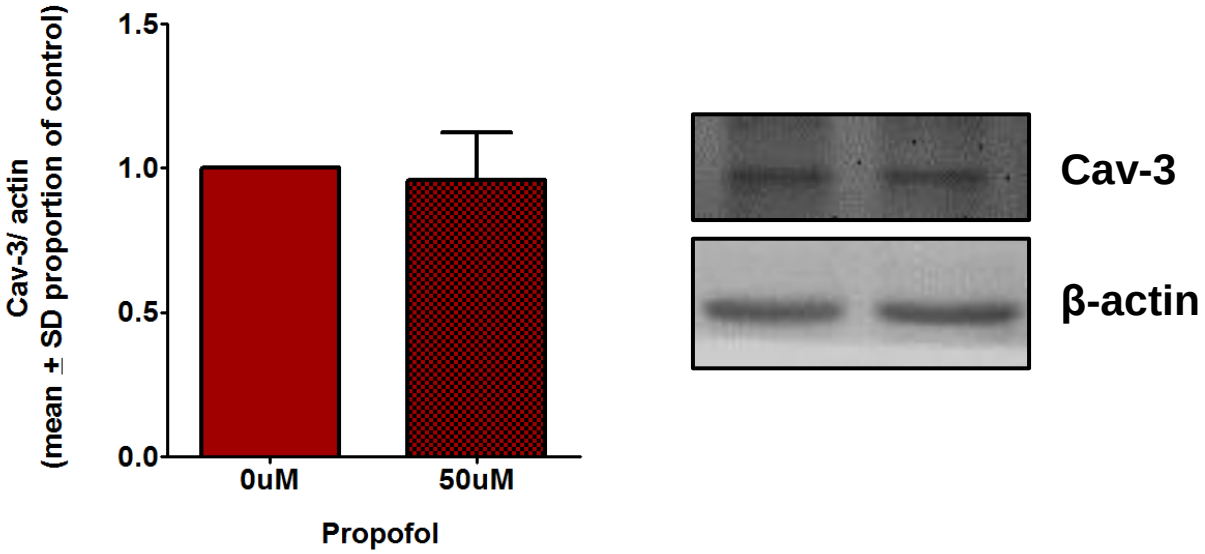

Figure 13. Cav-3 whole cells levels do not change with propofol treatment.
H9c2 cells were treated with 50µM propofol, and whole cell lysate Cav-3 levels determined using Western blot. n = 4.

Chapter 5: Discussion

5.1 ETAR inhibition decreases phosphorylated STAT3 Y705

In this study, STAT3 phosphorylation (Y705 and S727) levels were both utilized as functional outcomes of propofol-mediated signaling, in keeping with our prior research approach. Inhibiting ETAR activity with PD156707 yielded insight into signaling events. Based on our results, the activation of STAT3 Y705 and S727 appear as distinct outcomes. PD156707 significantly decreased levels of pSTAT3 Y705 relative to experimental control (10, 15μM), and relative to the propofol treatment group (5, 10, and 15μM), indicative of ETAR dependence. This contrasts significantly with the response of STAT3 S727 under the same experimental conditions. STAT3 S727 phosphorylation levels did not significantly change in response to ETAR inhibition. (Albeit non-significant statistically, pSTAT3 S727 followed a trend of increase in response to ETAR inhibition). A novel role for receptor biology in propofol mediated cellular adaptation is established. Our results suggest serine and tyrosine STAT3 phosphorylation events are independent — different phosphorylation agents, and different subsequent functions.

Certain activated receptors may directly phosphorylate STAT3 Y705 [124]. Alternatively, if they lack kinase ability, they recruit, and activate receptor tyrosine kinases [124]. The receptor tyrosine kinase in turn, phosphorylate STAT3 Y705 [124]. Phosphorylation of the tyrosine enables STAT3 homodimerization [104,124]. The homodimer binds to specific DNA sequences

and activates transcription [104]. STAT3 is a transcription factor for many proteins involved in cell growth and survival, including members of the anti-apoptotic BCl class [103,125].

Conversely, S727 phosphorylation involves ERK-dependent (involving MAPK kinases) and ERK independent mechanisms [126]. Phosphorylation of both S727 and Y705 residues allows maximal transcription activity [124,127]. Beyond, transcriptional control, pSTAT3 S727 also performs an important role in mitochondrial stabilization [103]. Serine phosphorylation targets STAT3 to the mitochondria, where it maintains integrity of complexes I and II of the electron transport chain [103]. Moreover, STAT3 presence in the mitochondria during ischaemia protects against mPTP [103].

The different routes of phosphorylation, as well as the different functions of the Y705 and S727 residues may explain the difference in behaviour of Y705 and S727 in response to ETAR inhibition. Our results are congruent with those of Banes-Berceli et al. (2007) that concluded that STAT3 Y705 phosphorylation occurred with ET-1 ligand application, dependent on ETAR [117]. In addition, Ogata et al. 2003 found that ETAR increased pSTAT3 in a receptor tyrosine kinase dependent manner [125]. The findings of these two studies are congruent with our own findings that propofol increases pSTAT3 Y705, and is unable to do so when the system is subjected to ETAR inhibition.

Although Banes-Berceli et al. (2007) documented an ETAR-related increase of pSTAT3 Y705, they did not examine pSTAT3 S727 levels [117]. In our study phosphorylation of S727 did not significantly change in response to stimuli. However, there was a trend towards

increased phosphorylation in response to ETAR inhibition or/ and propofol treatment. The increasing trend could be due to complex counter-regulatory systems present in cells. First, pSTAT3 Y705 is a negative regulator of pSTAT3 S727 [128]. Thus, it is expected when pSTAT3 Y705 decreases, pSTAT3 has a greater probability of increasing. Furthermore, there are ERK dependent and independent mechanisms of STAT3 S727 phosphorylation [126]. Many studies document that ETAR activation activates ERK [118,129,130]. However, there are experimental conditions under which ETAR does not activate ERK [129]. Moreover, Ogata et al. (2003) found that ETAR-dependent antiapoptotic effects while receptor tyrosine kinase dependent, were MAPK/PKC/ERK independent [125]. The ERK-MAPK and the PI3K-AKT pathways form a complex feedback loop, with both cross-activating and cross-inhibiting properties[131,132]. Paradoxically, ERK has both been implicated in inhibiting AKT, as well as increasing phosphorylation of STAT3 S727 [126,131]. Despite the statistically non-significant increases in pSTAT3 S727 in response to ETAR inhibitors, the residue could still be regulated by regulatory feedback loops.

Dr. Ansley and colleagues have previously shown that propofol increases activation of the components of the SAFE pathway (e.g. STAT3), and components of the RISK pathway (e.g. PI3K, and AKT) [77,79,97]. (The RISK and SAFE pathways are important components of protective conditioning cascades that alleviate cardiac ischaemia-reperfusion injury [95]). Moreover we have previously documented the existence of RISK-SAFE pathway crosstalk [97]. Our study provides further evidence of SAFE pathway involvement, possibly through the activation of receptor tyrosine kinases such as JAK2 (since the results support an ETAR mediated modulation of STAT3 Y705).

Taken together, this portion of the study supports propofol-mediated signaling possessing ETAR-dependent components.

5.2 Lipid raft disruption does not decrease phosphorylated STAT3 Y705

Methyl-β-cyclodextrin is commonly used to ascertain the dependence of cellular events upon the presence of intact lipid rafts [105,133,134]. Methyl-β-cyclodextrin is a cyclic oligosaccharide that has the ability to sequester cholesterol into its cavity from the plasma membrane [133]. The removal of cholesterol, a key component of lipid rafts, results in their dispersion. As a result cell viability is reduced and pathways such as AKT are reduced [135]. However, there are also signaling pathways which are upregulated with cholesterol depletion such as those involving ERK [136].

In our current study, propofol-mediated pSTAT3 Y705 signaling occurred despite cholesterol depletion with methyl-β-cyclodextrin. Our results suggest that propofol's effects do not require the presence of intact lipid rafts since lipid raft depletion did not result in a loss of signal (**Figure 3**). This result could be interpolated to include caveolae, as caveolae are a subtype of lipid raft.

Lipid raft disruption generally has deleterious cellular effects. Methyl-β-cyclodextrin in addition to inhibiting caveolar-dependent endocytosis, decreases clathrin-mediated

endocytosis by flattening clathrin-coated pits [137]. Thus, it is significantly interesting that this particular signaling mechanism remains intact.

Two main explanations are possible — the first stems from the possibility that propofol indirectly activates ETAR, through its effects on the membrane, and the second through the possibility that propofol is directly interacting and activating ETAR. In accordance with the first, propofol may be stabilizing lipid rafts, and countering the destabilizing effect of cholesterol depletion. In addition, a synergistic mechanism potentially could exist between methyl-β-cyclodextrin and propofol. The combination of methyl-β-cyclodextrin and propofol may be creating a membrane disruption that results in a more potent signal occurring.

Alternatively, ETAR endocytosis may be shifting from caveolae-dependent to caveolae-independent internalization mechanisms with propofol treatment. Upon ligand (ET-1) binding the ETA receptor internalizes [138]. Two types of internalization mechanisms have been noted for ETAR — clathrin-mediated endocytosis, and caveolae-dependent endocytosis[138–142]. The route taken may depend on cell type; although both mechanisms have been reported to occur in Chinese hamster ovary (CHO) cells [138]. In CHO cells, the prevalent ETAR endocytic pathway is caveolae-mediated, but the endocytic mechanism shifts to clathrin-dependent endocytosis when cholesterol is oxidized by cholesterol oxidase [138]. Additionally, keeping in mind that methyl-β-cyclodextrin also partially disrupts clathrin-mediated endocytosis, it is possible that ETAR is continuing to be endocytosed in a clathrin and caveolae independent manner. Certain receptor-binding proteins (Cholera toxin, ricin, Shiga toxin) use caveolae as a major route of cellular entry [143]. However, when clathrin and

caveolae-mediated endocytosis is inhibited, cellular uptake of these proteins remains, and is even increased in some cases [143]. Thus even though, methyl-β-cyclodextrin disrupts caveolae, the cell has contingency mechanisms in the form of clathrin-coated pits, and other endocytic mechanisms, guaranteeing ETAR internalization.

5.3 AKT interacts with ETAR; Propofol does not alter AKT cellular distribution

AKT localizes to the plasma membrane, via docking with PIP3, for activation [98]. Furthermore, modulation, and differential localization of AKT occurs in certain signaling contexts [144]. For example, Gonzalez and McGraw (2009) found that an isoform of AKT increased at the plasma membrane in response to insulin. Furthermore, if this phenomenon was prevented, key insulin signaling events could no longer occur to the same capacity [144]. Moreover, AKT is a component of the RISK pathway and interacts directly with ETAR [122].

Our findings that AKT co-immunoprecipitates with ETAR are consistent with previous work of Chung and Walker (2007) [122]. Additionally, the ETAR-AKT interaction was not lost with propofol treatment. Moreover, our immunofluorescence results indicated that cellular AKT intensity levels did not change. Our results suggest that AKT interaction with the cellular membrane, and localization were not altered by propofol treatment. This is important given that previous studies report AKT phosphorylation as a factor in propofol-mediated signaling[79,97]. Perhaps the AKT activation that accompanies propofol treatment is manifested solely via the increase in its phosphorylated state and not concurrent localization and expression level changes.

5.4 Propofol increases intracellular levels of ETAR

Key findings from our study included ETAR detection in intracellular puncta and a significant increase in intracellular levels of ETAR in response to 50μM of propofol (See **Figure 8**).

When endothelin receptors are activated by a ligand, the receptors are subsequently internalized, and either recycled back to the surface or sent to lysosomal compartments to be degraded [139]. Two major factors could have contributed to the increased pool of intracellular vesicular ETAR. Firstly, internalized ETAR, prior to degradation/ recycling is present. Secondly, there could have been an increase in newly synthesized ETAR being shuttled to the cellular surface. Our immunofluorescence studies indicated that ETAR intensity was unchanged near the plasma membrane. This could indicate that the rate of ETAR internalization was in equilibrium with new/ recycled ETAR reaching the cellular surface.

5.5 ETAR and Cav-1 colocalize close to the level of the plasma membrane

Our study characterized extensive ETAR-Cav-1 colocalization at the plasma membrane (**Figure 8A**) as opposed to intracellularly (**Figure 7A**). Intracellularly there was a diminutive amount of ETAR and Cav-1 immunofluorescence overlap.

At the cellular surface Cav-1 and ETAR are in close proximity, which can be explained by ETAR enrichment in caveolae [6]. Our immunofluorescence data suggests that Cav-1 did not

follow ETAR internalization in response to stimulation with propofol. This contrasts distinctly to the preliminary response of Cav-3 as it colocalizes extensively intracellularly (**Figure 14**).

The possibility of ETAR tracking inside the cell with Cav-3 but not with Cav-1 may suggest that Cav-1 and Cav-3, (although both are scaffolding proteins of caveolae), have different roles.

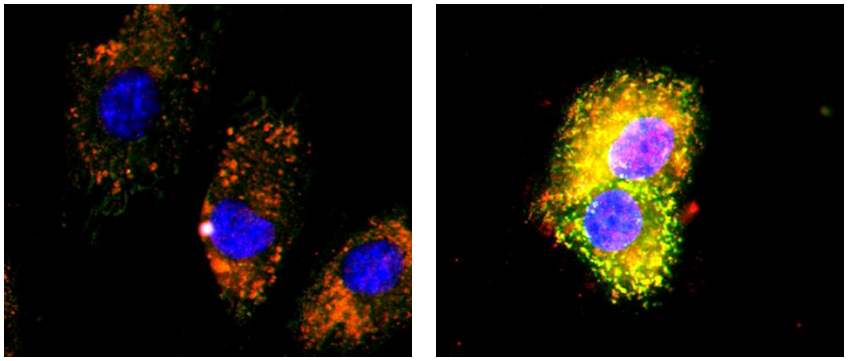

Figure 14. Extensive Cav-3 – ETAR colocalization occurs intracellularly.
Cells were treated as per standard protocol, fixed, and completely permeabilized. Cells were stained for ETAR (green), Cav-3 (red), and nuclei (blue, Hoechst) and visualized using immunofluorescence. The merged image of all 3 channels is presented.

5.6 Caveolae largely undisturbed by propofol

Although the possibility of propofol presence disturbing lipid rafts cannot be discounted, this study provides support to the contrary. As seen in **Figure 9** buoyant light fractions that

correspond to lipid rafts and caveolae fractions were present in both control conditions and in response to treatment with 25μM or 50μM of propofol. Furthermore, these light fractions contained similar distributions of Cav-1 between conditions. If propofol was a major disruptor of lipid rafts, then these light fractions would have been eliminated, and Cav-1 distribution would have shifted to lower, bulk/ cytosolic fractions.

As previously mentioned, propofol did not alter Cav-1's, cellular distribution. Furthermore, Cav-1 whole cell levels remained unchanged with propofol treatment. Additionally, propofol did not alter Cav-1 protein levels as visualized by both partially and completely permeabilized immunofluorescent conditions. Moreover, propofol failed to alter Cav-1 lipid raft cellular distribution. Altogether, Cav-1 localization, and in turn caveolae presence, were unaltered with propofol treatment. However, as discussed above propofol did affect Cav-3 distribution.

5.7 Propofol: A potential modulator of Cav-3

Cardiomyocytes, are special in that they contain all three isoforms of caveolin — Cav-1, Cav-2, and Cav-3 [17]. The importance of Cav-3 has been well documented, in that overexpression is protective, and mice carrying knock out mutations of Cav-3 have dysfunctional cardiac phenotypes [106].

In H9c2 cells, we observed that Cav-3 differentially distributed intracellularly as compared to Cav-1 (**Figure 7A, Figure 12**). Additionally, the earlier touched upon Cav-3 — ETAR

intracellular colocalization provides further support for existence of differential Cav-1 and Cav-3 behaviour. Although, Cav-3 whole cell lysates followed the same pattern as was seen by Cav-1, and remained constant with propofol administration, Cav-3 nuclear localization increased with 50μM propofol treatment.

We were not the only ones to report changes in Cav-3 localization in response to a stimulus. Ballard-Croft et al (2006) reported that ischaemia-reperfusion redistributed Cav-3 to cytosolic fractions (using discontinuous sucrose fractionation)[106]. Furthermore, Cav-3 redistributes to cytoplasmic components in a form of cardiac hypertrophy [107]. Jeong et al. (2009) induced cardiac hypertrophy by treating cardiomyocytes with one of two catecholamines — isoproterenol or phenylephrine. Under these conditions of catecholamine-induced hypertrophy Cav-3 whole cell lysate levels remained uniform, while Cav-3 localization changed [107]. As seen by discontinuous fractionation, Cav-3 decreased in the membrane, and increased in the bulk/ cytoplasmic components [107]. Moreover, the level of Cav-3 seemed to increase in the nuclear/ perinuclear region [107].

Thus Cav-3 may have a functionally important role of acting as a chaperone in cardioprotective signal transduction.

5.8 Signalosome

Conventionally, receptor binding leads to activation, which in turn activates signaling moieties dissolved and diffused within the cytoplasm [145,146]. However, although rapid

signaling events do occur in the vicinity of the plasma membrane, these constitute only the initial stages [145,146]. Some receptors do not undergo degradation immediately upon internalization or recycle back to the cellular surface. Instead, the receptors, in their internalised state undergo signal propagation/ initiation events [145]. Indeed, some receptor-mediated signaling can first originate from the endosome [145].

The signalosome is an endosomal compartment that contains a cluster of signaling moieties[145]. Docking happens with receptor internalization between its vesicle and a signalosome. Interaction between receptor and signalosome depends on method of internalization (**Illustration 2**) [145]. For example, transforming growth factor beta (TGF-β) interacts, and activates different sets of signals through a signalosome, depending on whether it was internalized using caveolae or if it was internalized with clathrin [145].

Boivin et al. (2005) investigated the possibility of clustering of endothelin signaling pathway components with caveolae components in the formation of a signalosome [140]. Using confocal immunofluorescent colocalization they determined that Cav-3 did not colocalize with components of the endothelin signaling pathway (including ETAR), save for G_{α} [140]. They concluded that caveosomes were not necessary for the endothelin signaling pathway [140]. However, the authors examined the localization under basal (i.e. unstimulated) conditions, without ET-1, or any other agonist present that could activate the signaling cascade. Thus, it is possible that a signalosome (lacking caveolar components) is formed, or even a caveolar signalosome.

Our immunofluorescent ETAR results depicted ETAR as cytoplasmic puncta (suggesting that ETAR was present in vesicles). Moreover, the intensity of intracellular ETAR immunofluorescence (corresponding to protein levels) significantly increased with 50μM propofol treatment. There is the distinct possibility that the vesicular ETAR is part of an internal signaling cascade interacting with/ forming signalosome compartments, which propagate the cellular signal. Subsequently, the ETAR is either recycled, or degraded. Besides ETAR, other proteins showed intracellular compartmental increases with propofol stimulation suggesting, a larger interacting, and signaling collective. Here we reported that Cav-3 increased in a nuclear/ perinuclear manner. Furthermore, our laboratory has previously shown that STAT3 also translocated to a perinuclear space with propofol treatment [97].

Thus, the nuclear translocation of ETAR and Cav-3 herein described is similar to nuclear factor kappa-light-chain-enhancer of activated B cells (NFκB) and STAT3 translocation in our previous published work [97]. Cav-3 may conceivably be acting as a chaperone for trafficking the signal intracellularly. Propofol may stimulate intracellular signal transduction by signalosome formation. This could be the mechanism of RISK-SAFE crosstalk which culminates in Bcl-2 upregulation and consequently cellular protection [97]. Taken together, our findings may be indirect evidence of drug mediated signalosome formation requiring our further study.

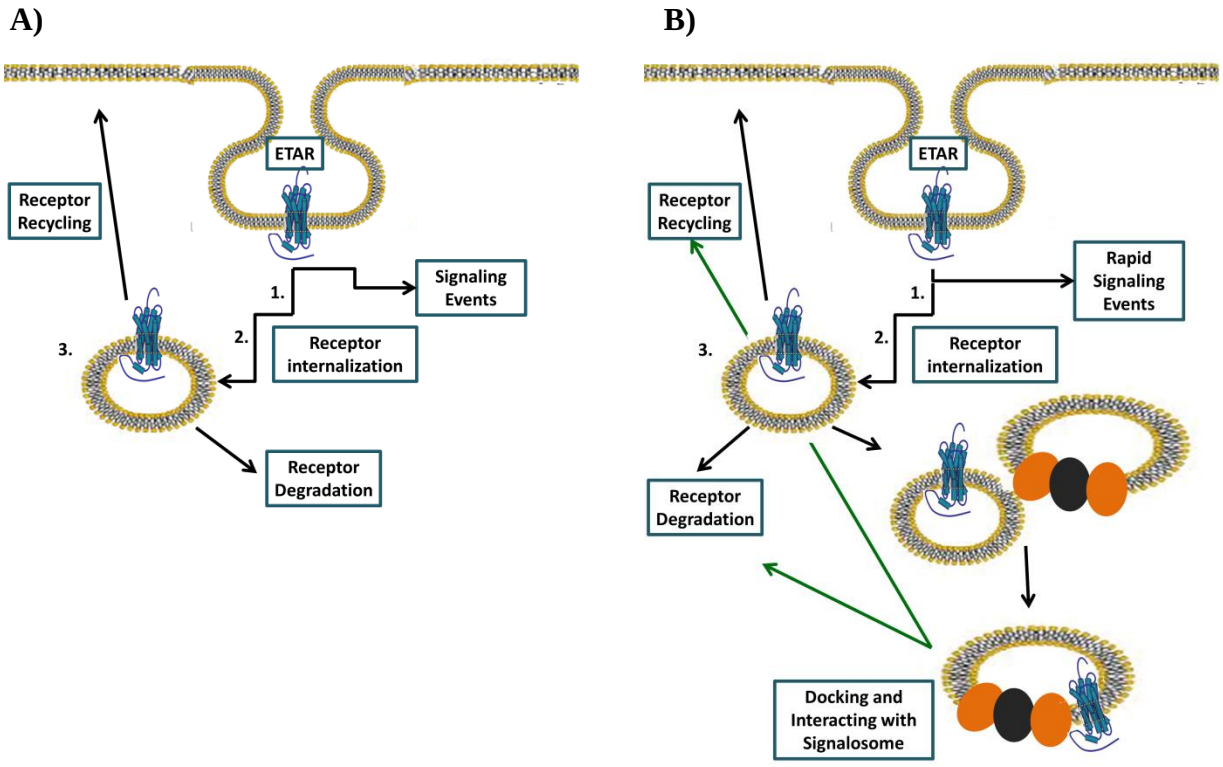

Illustration 2. Conventional signaling vs. the signalosome.
A) Traditionally, signaling events occur, the receptor is internalized and processed by the cell. **B)** Signalosome theory postulates that internalized receptors can continue to signal as they dock and interact with endosomal signalosome complexes (that contain clusters of signaling moieties).

5.9 Propofol has a mild permeabilizing effect

To examine the influence of propofol on membrane permeability and to confirm the mildly permeabilizing effect of paraformaldehyde, GM130, an intracellular marker was immunofluorescently visualized in cells (**Figure 15**).

Propofol has a mild permeabilizing effect as can be seen in top panels of **Figure 15**. However, propofol has no further permeabilizing effect on cells treated with triton (bottom

panels). The mild propofol permeabilization effect would not have created a significant artifact in previous immunofluorescent results. Cav-1 distribution within the cell was measured by both immunofluorescence and discontinuous sucrose fractionation. Had the artifact been sufficiently large to alter results, then the immunofluorescence and discontinuous sucrose fractionation results would have differed from each other. Rather these methods indicated respectively, that there was no change in Cav-1 localization near the membrane, or in lipid rafts. It is interesting that propofol mildly permeabilizes the membrane as this is a similar to the effect of phenol on prokaryotic membranes [147,148].

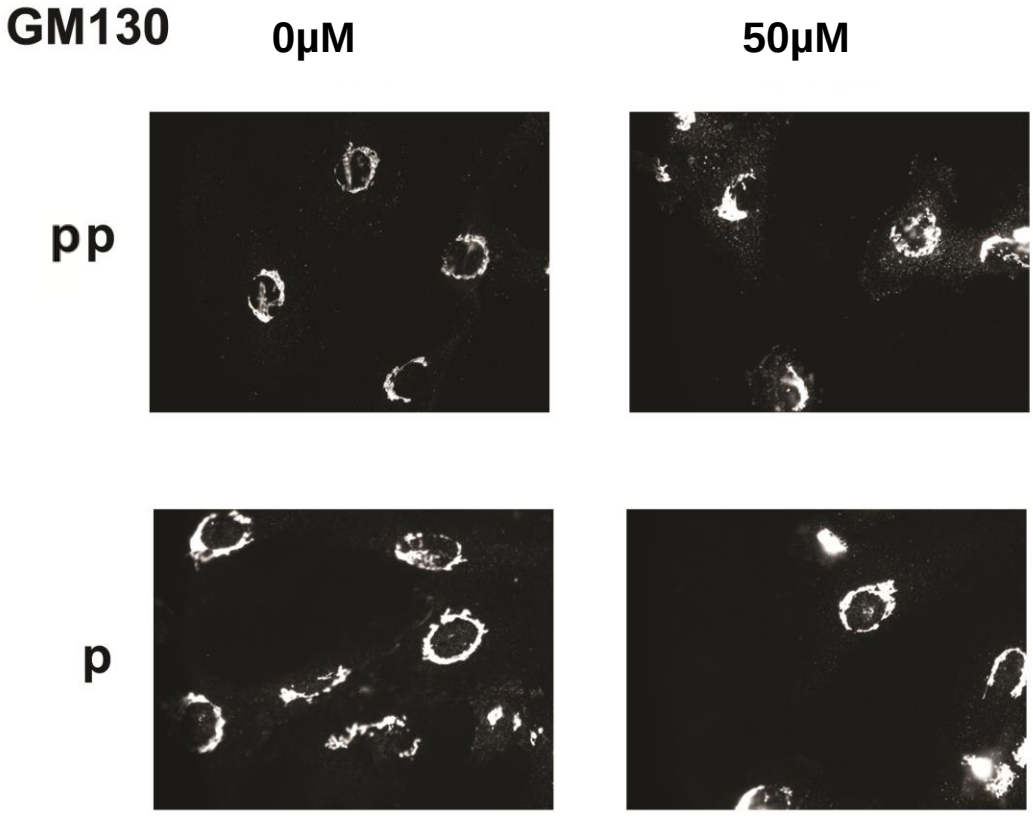

Figure 15. Propofol mildly permeabilizes the partially permeabilized condition. Cells were control or propofol (50μM) treated as indicated in the top row. pp represents partially permeabilized conditions (permeabilization solely as a results of 4% paraformaldehyde fixation), and p represents completely permeabilized conditions (Cells treated with 0.2% Triton detergent, subsequent to paraformaldehyde fixation). Cells were stained with GM130, a Golgi apparatus marker. Representative images from two experimental repeats.

5.10 Summary of significant results: ETAR

Inhibition of ETAR resulted in a decrease of pSTAT3 Y705. In addition, propofol application increased intracellular ETAR protein levels. Taken together, these results support the idea that propofol-mediated signaling was in part dependent on ETAR.

5.11 Summary of significant results: Caveolae

STAT3 Y705 activation occurred in response to propofol despite cholesterol depletion with methyl-β-cyclodextrin. The former statement suggests that propofol-mediated STAT3 modulation is not dependent on intact caveolae. However, despite this, propofol seems to be modulating Cav-3 localization. Cav-3 increased in the nucleus with propofol treatment. See **Illustration 3** for a summary of results.

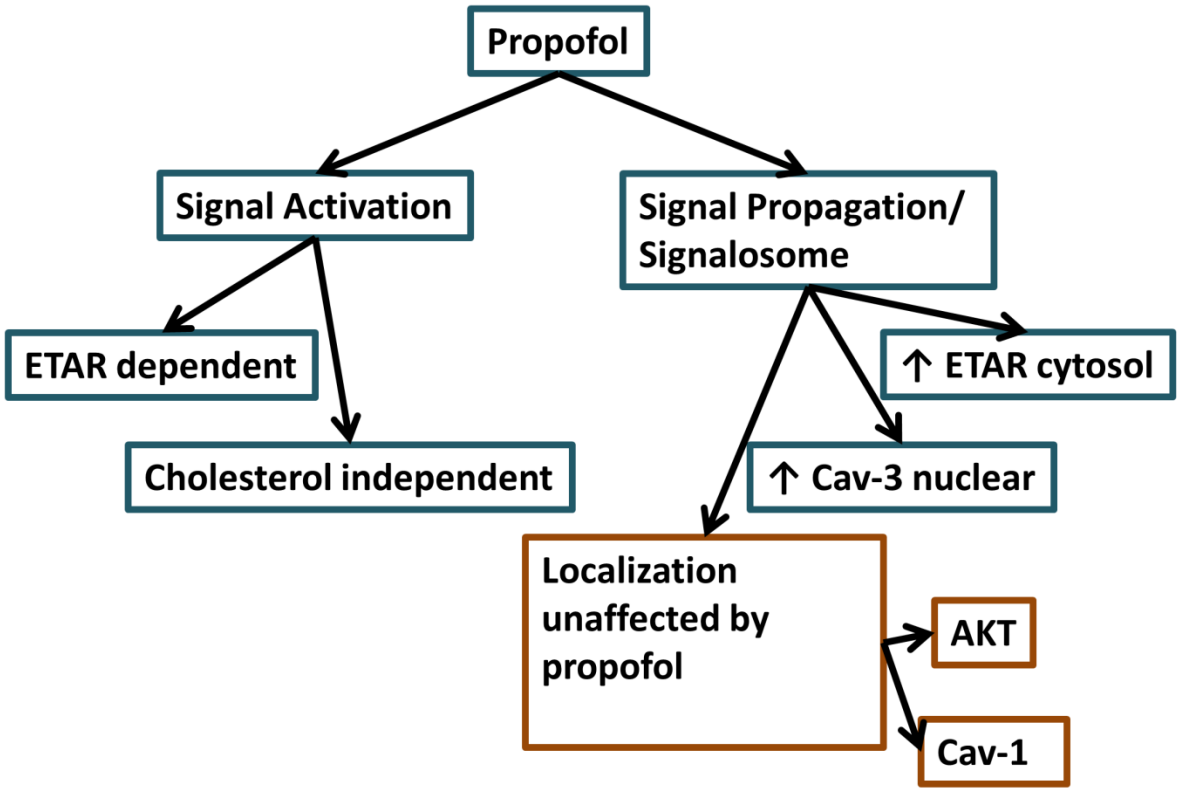

Illustration 3. Main results summary.
Propofol-mediated signaling is partially ETAR dependent. Additionally, propofol-mediated signaling is cholesterol- independent. ETAR increases intracellularly, Cav-3 increases in the nucleus. AKT and Cav-1 localizations are unaffected by propofol-mediated signaling.

Chapter 6: Conclusion

6.1 General Discussion

Myocardial ischaemia-reperfusion injury and its sequelae is a serious problem, especially in high risk patients during surgery. Current conditioning strategies for mitigation of the injury and its consequences have not translated into clinical effectiveness. The general anesthetic, propofol, is showing promise as an alternative pharmacological agent against detrimental ischaemia-reperfusion effects [83]. Our laboratory has previously shown that propofol protects the heart during open heart surgery [83]. Propofol's antioxidant abilities are a minor adjunct to its protective effect, as propofol also activates the cardioprotective RISK and SAFE pathways [97].

Herein we investigated the dependence and influence of propofol-mediated signaling on ETAR and caveolae. Indeed, propofol activates and modulates ETAR. As for propofol's effect and dependence on caveolae, the results were mixed. Propofol-mediated signaling does not seem to be dependent on intact caveolae. Furthermore, Cav-1 distribution is unaffected, and Cav-1 only minutely colocalizes with the ETAR intracellularly. However, Cav-3 increases in the nucleus with propofol treatment. Taken together, the propofol-mediated signaling pathway can partially be initiated at the ETAR receptor, and causes inward cellular movement of ETAR and Cav-3.

Our work introduces ETAR as a novel target of propofol. The receptor and its ligands may be of therapeutic value to target for the enabling of cardioprotection. Moreover, ETAR agonists and antagonists are already being looked at for their potential in modulating cardiac injury. Overall, investigating cellular membrane targets and modulators of propofol-mediated signaling is important in the context of further ischaemia-reperfusion cardiac injury prevention.

6.2 Limitations

Our results are not directly translatable to clinical scenarios due to the nature and model of the study. The H9c2 cell line is a good representation of cardiac cells. However, this work has not been translated into isolated-heart or in vivo animal models for testing. We did not test a model of ischaemia-reperfusion injury. Future potential work could involve testing the propofol-mediated signaling model on in vivo ischaemia-reperfusion injury models.

Furthermore, the biological system is a dynamic one. Documenting the effect of propofol at 30 minutes only offers a limited glimpse into the workings of the system. Some cellular signaling events occur much more rapidly than the 30 minutes time point that was used. Additionally, other cellular signaling events take much longer, especially when factoring in the time for transcription to be altered, and then those proteins to be subsequently made. However, 30 minutes is a good time point to look at in terms of STAT-3 signaling, as maximal phosphorylation occurs at this point [97].

ETAR inhibition was investigated solely with an ETAR selective inhibitor, PD156707. There is the potential that PD156707 has off-target effects outside of its ETAR inhibitory activity. However, use of this inhibitor has been well documented, and any auxiliary unintended effects have yet to be noted [149,150].

Propofol is a small hydrophobic molecule. As such it may be subject to potential uptake into the cavity of methyl-β-cyclodextrin. Thus, if this were the case, propofol treatment following 30 minutes of pre-incubation with methyl-β-cyclodextrin, may have the same effect as treating with an excess of cholesterol. Although some cells (~20% under control conditions) detach and die after the extended methyl-β-cyclodextrin exposure, the state of the lipid rafts was not formally assessed. This can be done by loading a discontinuous sucrose gradient with sample, and determining how much of the Cav-1 protein population has migrated to bulk/ cytosolic components. As a confirmatory study, the experiment can be repeated with other inhibitors of lipid rafts such as filipin and nystatin.

In combination methyl-β-cyclodextrin and 50μM propofol increased levels of pSTAT3 Y705. However, it is impossible to delineate whether this is due to the presence of propofol, or the methyl-β-cyclodextrin – propofol combination. Although pSTAT3 Y705 of the combination group was significantly greater than control, it was not significantly greater than the propofol alone nor methyl-β-cyclodextrin alone.

Co-immunoprecipitation does not necessarily measure direct interaction between proteins. For one, the protein of interest may be part of the complex that immunoprecipitates, but not in direct interaction with the other protein of interest. Alternatively, the interaction may be spurious, and a result of non-specific interactions, leading to a false documentation of an interaction.

Immunofluorescent colocalization can also create artifacts. That, which is seen as an overlap, merely represents the two proteins present in the same voxel. They may be merely in close proximity, and not directly interacting with one another.

Using an alkaline (detergent-free) carbonate buffer to lyse cells and subsequently subject them to a discontinuous sucrose fractionation, overcomes problems associated with detergent-related artifacts. However, this method also has the potential of the creation of minor extraction artifacts — namely, some non-lipid-raft associated proteins may become incorporated, and lipid rafts may become contaminated with other membranes following lysis and sonication [142,151,152].

6.3 Future directions

One possible avenue of future research is to continue investigating the role of ETAR, and other membrane receptors, but in a model of ischaemia-reperfusion injury. It does not necessarily need to be an in vivo ischaemia-reperfusion injury model, but can be an in vitro

cellular assay where cells are treated with propofol following an acute insult (for example, H_2O_2 injury; simulated ischaemia-reperfusion injury).

Furthermore, propofol's effect on physical membrane properties warrants further investigation. As mentioned in the introduction, it has already been documented that propofol alters biophysical properties of the cellular membrane, such as the critical phase transition temperature. Furthermore, we have preliminarily seen that propofol increases membrane permeability. The next immediate step would be to treat cells with a range of propofol concentrations, to determine if the effect is propofol concentration dependent.

As previously mentioned ERK influences the RISK and SAFE pathways, but its role is yet to be elucidated [126,131]. Due to the interconnected nature of ERK, determining whether it plays an integral role in propofol mediated signaling is an important subsequent experimental approach. This could potentially pave the way to discovering further involvement of the MAPK system within the context of propofol-mediated signaling.

6.4 Clinical relevance

Propofol protects the heart from ischaemia-reperfusion injury [120]. Moreover, this protection extends to the population with diabetes, which cannot be said for other cardioprotective strategies [120]. The current study documented the occurrence of propofol-mediated signaling despite lipid raft disruption, which is analogous to patients using statins. Propofol remains a

potential alternative avenue of protection against ischaemia-reperfusion injury, but more study is required.

Pathway corruption due to lipid raft disruption is a major limitation in other cardioprotective paradigms. Cholesterol depletion results are of relevance to the general population, as many people are taking statins (which deplete cholesterol). It is significant that propofol is not dependent on the presence of cholesterol to activate protective signaling cascades.

Society is gradually attempting to move towards an age of personalized medicine. It is impossible to uniformly treat individual patients and expect the same outcome when there is an extensive amount of biological variability between individuals. Variation in genetics, proteomics, epigenetics, disease states, and even age contribute to the variability in bodily reactions to pharmacological intervention.

Mapping where propofol exerts its effects on a cellular level has further health relevance. Firstly, elucidating the primary target of action opens the possibility of discovery for other pharmacological mimics to be developed and applied to achieve the same end — cardioprotection. Current protective strategies are not sufficient, especially as they are not effective in all population groups. Secondly, knowing a patient's protein signature, and which pathways may be underactive would be useful in determining whether treating with propofol would be beneficial during their surgery. Many altered physiological states — certain diseases, and even aging experience maladaptive activation of signaling cascades.

In summary, this study has provided a potential protective propofol target — ETAR. Additionally, it makes a small step in the direction of a personalized medicine initiative.

References

1. McMullen, T. P. W., Lewis, R. N. a H. & McElhaney, R. N. Cholesterol-phospholipid interactions, the liquid-ordered phase and lipid rafts in model and biological membranes. *Curr. Opin. Colloid Interface Sci.* **8,** 459–468 (2004).

2. Singer, S. J. & Nicolson, G. L. The fluid mosaic model of the structure of cell membranes. *Science* **175,** 720–731 (1972).

3. Connor, J., Bucana, C., Fidler, I. J. & Schroit, a J. Differentiation-dependent expression of phosphatidylserine in mammalian plasma membranes: quantitative assessment of outer-leaflet lipid by prothrombinase complex formation. *Proc. Natl. Acad. Sci. U. S. A.* **86,** 3184–3188 (1989).

4. Leventis, P. a & Grinstein, S. The distribution and function of phosphatidylserine in cellular membranes. *Annu. Rev. Biophys.* **39,** 407–427 (2010).

5. Prinetti, A., Chigorno, V., Tettamanti, G. & Sonnino, S. Sphingolipid-enriched membrane domains from rat cerebellar granule cells differentiated in culture. A compositional study. *J. Biol. Chem.* **275,** 11658–11665 (2000).

6. Pike, L. J. Lipid rafts: bringing order to chaos. *J. Lipid Res.* **44,** 655–667 (2003).

7. Sonnino, S., Mauri, L., Chigorno, V. & Prinetti, A. Gangliosides as components of lipid membrane domains. *Glycobiology* **17,** 1R–13R (2007).

8. De Almeida, R. F. M., Fedorov, A. & Prieto, M. Sphingomyelin/phosphatidylcholine/cholesterol phase diagram: boundaries and composition of lipid rafts. *Biophys. J.* **85,** 2406–2416 (2003).

9. Scheiffele, P., Roth, M. G. & Simons, K. Interaction of influenza virus haemagglutinin with sphingolipid-cholesterol membrane domains via its transmembrane domain. *EMBO J.* **16,** 5501–5508 (1997).

10. Simons, K. & Ikonen, E. Functional rafts in cell membranes. *Nature* **387,** 569–572 (1997).

11. Simons, K. & Toomre, D. Lipid rafts and signal transduction. *Nat. Rev. Mol. Cell Biol.* **1,** 31–39 (2000).

12. M'Baye, G., Mély, Y., Duportail, G. & Klymchenko, A. S. Liquid ordered and gel phases of lipid bilayers: fluorescent probes reveal close fluidity but different hydration. *Biophys. J.* **95,** 1217–1225 (2008).

13. Ahmed, S. N., Brown, D. a. & London, E. On the origin of sphingolipid/cholesterol-rich detergent-insoluble cell membranes: Physiological concentrations of cholesterol and sphingolipid induce formation of a detergent-insoluble, liquid-ordered lipid phase in model membranes. *Biochemistry* **36,** 10944–10953 (1997).

14. Kim, S. Il, Yi, J. S. & Ko, Y. G. Amyloid beta oligomerization is induced by brain lipid rafts. *J. Cell. Biochem.* **99,** 878–889 (2006).

15. Viola, A. & Gupta, N. Tether and trap: Regulation of membrane-raft dynamics by actin-binding proteins. *Nat. Rev. Immunol.* **7,** 889–896 (2007).

16. Head, B. P., Patel, H. H. & Insel, P. a. Interaction of membrane/lipid rafts with the cytoskeleton: Impact on signaling and function: Membrane/lipid rafts, mediators of cytoskeletal arrangement and cell signaling. *Biochim. Biophys. Acta - Biomembr.* **1838,** 532–545 (2014).

17. Head, B. P. *et al.* Microtubules and actin microfilaments regulate lipid raft/caveolae localization of adenylyl cyclase signaling components. *J. Biol. Chem.* **281,** 26391–26399 (2006).

18. Schilling, J. M., Roth, D. M. & Patel, H. H. Caveolins in cardioprotection - translatability and mechanisms. *Br. J. Pharmacol.* **172,** 2114–2125 (2015).

19. Parton, R. G. & Simons, K. The multiple faces of caveolae. *Nat. Rev. Mol. Cell Biol.* **8,** 185–194 (2007).

20. Fujita, T. *et al.* Caveolin-3 inhibits growth signal in cardiac myoblasts in a Ca 2+-dependent manner. *J. Cell. Mol. Med.* **10,** 216–224 (2006).

21. Salani, B., Briatore, L., Garibaldi, S., Cordera, R. & Maggi, D. Caveolin-1 down-regulation inhibits insulin-like growth factor-I receptor signal transduction in H9c2 rat cardiomyoblasts. *Endocrinology* **149,** 461–465 (2008).

22. Palade, G. Fine structure of blood capillaries. *J. Appl. Phys.* **24,** 1424–1436 (1953).

23. Yamada, E. The fine structure of the gall bladder epithelium of the mouse. *J. Biophys. Biochem. Cytol.* **1,** 445–458 (1955).

24. Mundy, D. I., Machleidt, T., Ying, Y., Anderson, R. G. W. & Bloom, G. S. Dual control of caveolar membrane traffic by microtubules and the actin cytoskeleton. *J. Cell Sci.* **115,** 4327–4339 (2002).

25. Rybin, V. O., Grabham, P. W., Elouardighi, H. & Steinberg, S. F. Caveolae-associated proteins in cardiomyocytes: caveolin-2 expression and interactions with caveolin-3. *Am. J. Physiol. Heart Circ. Physiol.* **285,** H325–H332 (2003).

26. Yamamoto, M., Okumura, S., Oka, N., Schwencke, C. & Ishikawa, Y. Downregulation of caveolin expression by cAMP signal. *Life Sci.* **64,** 1349–1357 (1999).

27. Niesman, I. R. *et al.* Caveolin isoform switching as a molecular, structural, and metabolic regulator of microglia. *Mol. Cell. Neurosci.* **56,** 283–297 (2013).

28. Capozza, F. *et al.* Muscle-specific interaction of caveolin isoforms: Differential complex formation between caveolins in fibroblastic vs. muscle cells. *Am. J. Physiol. Cell Physiol.* **288,** C677–C691 (2005).

29. Stahlhut, M. & van Deurs, B. Identification of filamin as a novel ligand for Caveolin-1: Evidence for the organization of Caveolin-1-associated membrane domains by the actin cytoskeleton. *Mol. Biol. Cell* **11,** 325–337 (2000).

30. Tsutsumi, Y. M. *et al.* Cardiac-specific overexpression of Caveolin-3 induces endogenous cardiac protection by mimicking ischemic preconditioning. *Circulation* **118,** 1979–1988 (2008).

31. Vallejo, J. & Hardin, C. D. Expression of caveolin-1 in lymphocytes induces caveolae formation and recruitment of phosphofructokinase to the plasma membrane. *FASEB J.* **19,** 586–587 (2005).

32. Bernatchez, P., Sharma, A., Bauer, P. M., Marin, E. & Sessa, W. C. A noninhibitory mutant of the caveolin-1 scaffolding domain enhances eNOS-derived NO synthesis and vasodilation in mice. *J. Clin. Invest.* **121,** 3747–3755 (2011).

33. Patel, H. H. & Insel, P. a. Lipid rafts and caveolae and their role in compartmentation of redox signaling. *Antioxid. Redox Signal.* **11,** 1357–1372 (2009).

34. Pelkmans, L., Püntener, D. & Helenius, A. Local actin polymerization and dynamin recruitment in SV40-induced internalization of caveolae. *Science* **296,** 535–539 (2002).

35. Shen, L. & Turner, J. R. Actin depolymerization disrupts tight junctions via caveolae-mediated endocytosis. *Mol. Biol. Cell* **16,** 3919–3936 (2005).

36. Kou, L., Sun, J., Zhai, Y. & He, Z. The endocytosis and intracellular fate of nanomedicines: Implication for rational design. *Asian J. Pharm. Sci.* **8,** 1–8 (2013).

37. Ecke, G. G. & Kolka, A. J. 2, 6-diisopropylphenol. (1966). at <http://www.google.ca/patents/US3271314>

38. Glen, J. B. & James, R. 2,6-Diisopropylphenol as an anaesthetic agent. (1977). at <https://www.google.ca/patents/US4056635>

39. James, R. & Glen, J. B. Synthesis, biological evaluation, and preliminary structure-activity considerations of a series of alkylphenols as intravenous anesthetic agents. *J. Med. Chem.* **23,** 1350–1357 (1980).

40. Glen, J. B. Animal studies of the anaesthetic activity of ICI 35 868. *Br. J. Anaesth.* **52,** 731–742 (1980).

41. Dye, D. & Watkins, J. Suspected anaphylactic reaction to Cremophor EL. *BMJ* **280,** 1353–1353 (1980).

42. Glen, J. B. & Hunter, S. C. Pharmacology of an emulsion formulation of ICI 35868. *BJA Br. J. Anaesth.* **57,** 836–836 (1985).

43. Harvey, K. A., Xu, Z., Pavlina, T. M., Zaloga, G. P. & Siddiqui, R. A. Modulation of endothelial cell integrity and inflammatory activation by commercial lipid emulsions. *Lipids Health Dis.* **14,** 9 (2015).

44. Zheng, L. *et al.* Intralipid decreases apolipoprotein M levels and insulin sensitivity in rats. *PLoS One* **9,** e105681 (2014).

45. Bahri, M. A. *et al.* Does propofol alter membrane fluidity at clinically relevant concentrations? An ESR spin label study. *Biophys. Chem.* **129,** 82–91 (2007).

46. Balasubramanian, S. V., Campbell, R. B. & Straubinger, R. M. Propofol, a general anesthetic, promotes the formation of fluid phase domains in model membranes. *Chem. Phys. Lipids* **114,** 35–44 (2002).

47. Tsuchiya, H. Structure-specific membrane-fluidizing effect of propofol. *Clin. Exp. Pharmacol. Physiol.* **28,** 292–299 (2001).

48. Momo, F., Fabris, S., Bindoli, A., Scutari, G. & Stevanato, R. Different effects of propofol and nitrosopropofol on DMPC multilamellar liposomes. *Biophys. Chem.* **95,** 145–155 (2002).

49. Hansen, A. H. *et al.* Propofol modulates the lipid phase transition and localizes near the headgroup of membranes. *Chem. Phys. Lipids* **175-176,** 84–91 (2013).

50. Lodish, H., Berk, A. & Zipursky, S. L. in *Mol. Cell Biol.* (W. H. Freeman, 2000). at <http://www.ncbi.nlm.nih.gov/books/NBK21583/>

51. Bandeiras, C., Serro, A. P., Luzyanin, K., Fernandes, A. & Saramago, B. Anesthetics interacting with lipid rafts. *Eur. J. Pharm. Sci.* **48,** 153–165 (2013).

52. Gray, E., Karslake, J., Machta, B. B. & Veatch, S. L. Liquid general anesthetics lower critical temperatures in plasma membrane vesicles. *Biophys. J.* **105,** 2751–2759 (2013).

53. Grim, K. J. *et al.* Caveolae and propofol effects on airway smooth muscle. *Br. J. Anaesth.* **109,** 444–453 (2012).

54. Eltzschig, H. K. & Eckle, T. Ischemia and reperfusion—from mechanism to translation. *Nat. Med.* **17,** 1391–1401 (2011).

55. Frank, a. *et al.* Myocardial ischemia reperfusion injury: From basic science to clinical bedside. *Semin. Cardiothorac. Vasc. Anesth.* **16,** 123–132 (2012).

56. Raedschelders, K., Ansley, D. M. & Chen, D. D. Y. The cellular and molecular origin of reactive oxygen species generation during myocardial ischemia and reperfusion. *Pharmacol. Ther.* **133,** 230–255 (2012).

57. Hearse, D. J., Maxwell, L., Saldanha, C. & Gavin, J. B. The myocardial vasculature during ischemia and reperfusion: a target for injury and protection. *J. Mol. Cell. Cardiol.* **25,** 759–800 (1993).

58. Jennings, R. B., Sommers, H. M., Smyth, G. A., Flack, H. A. & Linn, H. Myocardial necrosis induced by temporary occlusion of a coronary artery in the dog. *Arch. Pathol.* **70,** 68–78 (1960).

59. Fliss, H. & Gattinger, D. Apoptosis in ischemic and reperfused rat myocardium. *Circ. Res.* **79,** 949–956 (1996).

60. Ansley, D. M. & Wang, B. Oxidative stress and myocardial injury in the diabetic heart. *J. Pathol.* **229,** 232–241 (2013).

61. Ma, S., Wang, Y., Chen, Y. & Cao, F. The role of the autophagy in myocardial ischemia/reperfusion injury. *Biochim. Biophys. Acta* **1852,** 271–276 (2014).

62. Linkermann, A. *et al.* Two independent pathways of regulated necrosis mediate ischemia-reperfusion injury. *Proc. Natl. Acad. Sci.* **110,** 12024–12029 (2013).

63. Matsui, Y. *et al.* Distinct roles of autophagy in the heart during ischemia and reperfusion: Roles of AMP-activated protein kinase and beclin 1 in mediating autophagy. *Circ. Res.* **100,** 914–922 (2007).

64. Gustafsson, Å. B. & Gottlieb, R. a. Autophagy in ischemic heart disease. *Circ. Res.* **104,** 150–158 (2009).

65. Kajstura, J. *et al.* Apoptotic and necrotic myocyte cell deaths are independent contributing variables of infarct size in rats. *Lab. Invest.* **74,** 86–107 (1996).

66. Qayumi, A. K. *et al.* The role of platelet-activating factor in regional myocardial ischemia-reperfusion injury. *Ann. Thorac. Surg.* **65,** 1690–1697 (1998).

67. Ansley, D. M. & Xia, Z. Propofol preservation of myocardial function in patients undergoing coronary surgery using cardiopulmonary bypass is dose dependent. *Anesthesiology* **98,** 1028–1029 (2003).

68. Heusch, G. Molecular basis of cardioprotection: Signal transduction in ischemic pre-, post-, and remote conditioning. *Circ. Res.* **116,** 674–699 (2015).

69. Lim, K. H. H., Halestrap, A. P., Angelini, G. D. & Suleiman, M.-S. Propofol is cardioprotective in a clinically relevant model of normothermic blood cardioplegic arrest and cardiopulmonary bypass. *Exp. Biol. Med. (Maywood).* **230,** 413–420 (2005).

70. Balyasnikova, I. V *et al.* Propofol attenuates lung endothelial injury induced by ischemia-reperfusion and oxidative stress. *Anesth. Analg.* **100,** 929–936 (2005).

71. Liu, K.-X., Rinne, T., He, W., Wang, F. & Xia, Z. Propofol attenuates intestinal mucosa injury induced by intestinal ischemia-reperfusion in the rat. *Can. J. Anaesth.* **54,** 366–374 (2007).

72. Shi, S., Yang, W., Chen, Y., Chen, J. & Tu, X. Propofol reduces inflammatory reaction and ischemic brain damage in cerebral ischemia in rats. *Neurochem. Res.* **39,** 793–799 (2014).

73. Xia, Z., Godin, D. V, Chang, T. K. . & Ansley, D. M. Dose-dependent protection of cardiac function by propofol during ischemia and early reperfusion in rats: effects on 15-F 2t -isoprostane formation. *Can. J. Physiol. Pharmacol.* **81,** 14–21 (2003).

74. Xia, Z., Godin, D. V. & Ansley, D. M. Propofol enhances ischemic tolerance of middle-aged rat hearts: Effects on 15-F2t-isoprostane formation and tissue antioxidant capacity. *Cardiovasc. Res.* **59,** 113–121 (2003).

75. Ye, L., Luo, C., McCluskey, S. A., Pang, Q. & Zhu, T. Propofol attenuates hepatic ischemia/reperfusion injury in an in vivo rabbit model. *J. Surg. Res.* **178,** e65–e70 (2012).

76. Yuzbasioglu, M. F., Aykas, A., Kurutas, E. B. & Sahinkanat, T. Protective effects of propofol against ischemia/reperfusion injury in rat kidneys. *Ren. Fail.* **32,** 578–583 (2010).

77. Wang, B., Luo, T., Chen, D. & Ansley, D. M. Propofol reduces apoptosis and up-regulates endothelial nitric oxide synthase protein expression in hydrogen peroxide-stimulated human umbilical vein endothelial cells. *Anesth. Analg.* **105,** 1027–1033 (2007).

78. Luo, T. *et al.* Propofol dose-dependently reduces tumor necrosis factor-alpha-induced human umbilical vein endothelial cell apoptosis: effects on Bcl-2 and Bax expression and nitric oxide generation. *Anesth. Analg.* **100,** 1653–1659 (2005).

79. Wang, B. *et al.* Propofol protects against hydrogen peroxide-induced injury in cardiac H9c2 cells via Akt activation and Bcl-2 up-regulation. *Biochem. Biophys. Res. Commun.* **389,** 105–111 (2009).

80. Ko, S. H. *et al.* Propofol attenuates ischemia-reperfusion injury in the isolated rat heart. *Anesth. Analg.* **85,** 719–724 (1997).

81. Kamada, N., Kanaya, N., Hirata, N., Kimura, S. & Namiki, A. Cardioprotective effects of propofol in isolated ischemia-reperfused guinea pig hearts: role of KATP channels and GSK-3beta. *Can. J. Anaesth.* **55,** 595–605 (2008).

82. Shirakawa, M., Imura, H. & Nitta, T. Propofol protects the immature rabbit heart against ischemia and reperfusion injury: Impact on functional recovery and histopathological changes. *Biomed Res. Int.* **2014,** 1–9 (2014).

83. Xia, Z., Huang, Z. & Ansley, D. M. Large-dose propofol during cardiopulmonary bypass decreases biochemical markers of myocardial injury in coronary surgery patients: A comparison with isoflurane. *Anesth. Analg.* **103,** 527–532 (2006).

84. Murry, C. E., Jennings, R. B. & Reimer, K. a. Preconditioning with ischemia: a delay of lethal cell injury in ischemic myocardium. *Circulation* **74,** 1124–1136 (1986).

85. Eckle, T. *et al.* Systematic evaluation of a novel model for cardiac ischemic preconditioning in mice. *Am. J. Physiol. Heart Circ. Physiol.* **291,** H2533–H2540 (2006).

86. Liu, Y. & Downey, J. M. Ischemic preconditioning protects against infarction in rat heart. *Am. J. Physiol.* **263,** H1107–H1112 (1992).

87. Clavien, P. A., Yadav, S., Sindram, D. & Bentley, R. C. Protective effects of ischemic preconditioning for liver resection performed under inflow occlusion in humans. *Ann. Surg.* **232,** 155–162 (2000).

88. Zaman, J. *et al.* Ischemic postconditioning provides cardioprotective and antiapoptotic effects against ischemia–reperfusion injury through iNOS inhibition in hyperthyroid rats. *Gene* **570,** 185–190 (2015).

89. Zhao, Z.-Q. *et al.* Inhibition of myocardial injury by ischemic postconditioning during reperfusion: comparison with ischemic preconditioning. *Am. J. Physiol. Heart Circ. Physiol.* **285,** H579–H588 (2003).

90. Loukogeorgakis, S. P. *et al.* Remote ischemic preconditioning provides early and late protection against endothelial ischemia-reperfusion injury in humans: Role of the autonomic nervous system. *J. Am. Coll. Cardiol.* **46,** 450–456 (2005).

91. Hausenloy, D. J. *et al.* Effect of remote ischaemic preconditioning on myocardial injury in patients undergoing coronary artery bypass graft surgery: a randomised controlled trial. *Lancet* **370,** 575–579 (2007).

92. Przyklenk, K., Bauer, B., Ovize, M., Kloner, R. A. & Whittaker, P. Regional ischemic 'preconditioning' protects remote virgin myocardium from subsequent sustained coronary occlusion. *Circulation* **87,** 893–899 (1993).

93. Andreadou, I., Iliodromitis, E. K., Koufaki, M. & Kremastinos, D. T. Pharmacological pre- and post- conditioning agents: reperfusion-injury of the heart revisited. *Mini Rev. Med. Chem.* **8,** 952–959 (2008).

94. Stadnicka, A., Marinovic, J., Ljubkovic, M., Bienengraeber, M. W. & Bosnjak, Z. J. Volatile anesthetic-induced cardiac preconditioning. *J. Anesth.* **21,** 212–219 (2007).

95. Lecour, S. Activation of the protective Survivor Activating Factor Enhancement (SAFE) pathway against reperfusion injury: Does it go beyond the RISK pathway? *J. Mol. Cell. Cardiol.* **47,** 32–40 (2009).

96. Suleman, N., Somers, S., Smith, R., Opie, L. H. & Lecour, S. C. Dual activation of STAT-3 and Akt is required during the trigger phase of ischaemic preconditioning. *Cardiovasc. Res.* **79,** 127–133 (2008).

97. Shravah, J. *et al.* Propofol mediates signal transducer and activator of transcription 3 activation and crosstalk with phosphoinositide 3-kinase/AKT. *JAK-STAT* **3,** e29554 (2014).

98. Hemmings, B. A. & Restuccia, D. F. PI3K-PKB/Akt pathway. *Cold Spring Harb. Perspect. Biol.* **4,** 1–4 (2012).

99. Perrelli, M.-G., Pagliaro, P. & Penna, C. Ischemia/reperfusion injury and cardioprotective mechanisms: Role of mitochondria and reactive oxygen species. *World J. Cardiol.* **3,** 186–200 (2011).

100. Wang, L. *et al.* Translocation of protein kinase C isoforms is involved in propofol-induced endothelial nitric oxide synthase activation. *Br. J. Anaesth.* **104,** 606–612 (2010).

101. Wang, H., Wang, G., Yu, Y. & Wang, Y. The role of phosphoinositide-3-kinase/Akt pathway in propofol-induced postconditioning against focal cerebral ischemia-reperfusion injury in rats. *Brain Res.* **1297,** 177–184 (2009).

102. Jatiani, S. S., Baker, S. J., Silverman, L. R. & Reddy, E. P. JAK/STAT pathways in cytokine signaling and myeloproliferative disorders: Approaches for targeted therapies. *Genes Cancer* **1,** 979–993 (2010).

103. Szczepanek, K., Chen, Q., Larner, A. C. & Lesnefsky, E. J. Cytoprotection by the modulation of mitochondrial electron transport chain: The emerging role of mitochondrial STAT3. *Mitochondrion* **12,** 180–189 (2012).

104. Liu, L., McBride, K. M. & Reich, N. C. STAT3 nuclear import is independent of tyrosine phosphorylation and mediated by importin-alpha3. *Proc. Natl. Acad. Sci. U. S. A.* **102,** 8150–8155 (2005).

105. Shah, M. Interactions of STAT3 with Caveolin-1 and heat shock protein 90 in plasma membrane raft and cytosolic complexes. Preservation of cytokine signaling during fever. *J. Biol. Chem.* **277,** 45662–45669 (2002).

106. Ballard-Croft, C., Locklar, A. C., Kristo, G. & Lasley, R. D. Regional myocardial ischemia-induced activation of MAPKs is associated with subcellular redistribution of caveolin and cholesterol. *Am. J. Physiol. Heart Circ. Physiol.* **291,** H658–H667 (2006).

107. Jeong, K., Kwon, H., Min, C. & Pak, Y. Modulation of the caveolin-3 localization to caveolae and STAT3 to mitochondria by catecholamine-induced cardiac hypertrophy in H9c2 cardiomyoblasts. *Exp. Mol. Med.* **41,** 226–235 (2009).

108. Patel, H. H. *et al.* Mechanisms of cardiac protection from ischemia/reperfusion injury: a role for caveolae and caveolin-1. *FASEB J.* **21,** 1565–1574 (2007).

109. Horikawa, Y. T. *et al.* Caveolin-3 expression and caveolae are required for isoflurane-induced cardiac protection from hypoxia and ischemia/reperfusion injury. *J. Mol. Cell. Cardiol.* **44,** 123–130 (2008).

110. Young, L. H., Ikeda, Y. & Lefer, A. M. Caveolin-1 peptide exerts cardioprotective effects in myocardial ischemia-reperfusion via nitric oxide mechanism. *Am. J. Physiol. Heart Circ. Physiol.* **280,** H2489–H2495 (2001).

111. Patel, H. H., Murray, F. & Insel, P. A. Caveolae as organizers of pharmacologically relevant signal transduction molecules. *Annu. Rev. Pharmacol. Toxicol.* **48,** 359–391 (2008).

112. Cantley, L. C. The phosphoinositide 3-kinase pathway. *Science (80-.).* **296,** 1655–1657 (2002).

113. Li, L., Ren, C. H., Tahir, S. A., Ren, C. & Thompson, T. C. Caveolin-1 maintains activated Akt in prostate cancer cells through scaffolding domain binding site interactions with and inhibition of serine/threonine protein phosphatases PP1 and PP2A. *Mol. Cell. Biol.* **23,** 9389–9404 (2003).

114. Schorlemmer, A., Matter, M. L. & Shohet, R. V. Cardioprotective signaling by endothelin. *Trends Cardiovasc. Med.* **18,** 233–239 (2008).

115. Shi-Wen, X. Endothelin-1 promotes myofibroblast induction through the ETA receptor via a rac/phosphoinositide 3-kinase/Akt-dependent pathway and is essential for the enhanced contractile phenotype of fibrotic fibroblasts. *Mol. Biol. Cell* **15,** 2707–2719 (2004).

116. Araki, M. *et al.* Endothelin-1 as a protective factor against beta-adrenergic agonist-induced apoptosis in cardiac myocytes. *J. Am. Coll. Cardiol.* **36,** 1411–1418 (2000).

117. Banes-Berceli, A. K. L. *et al.* Angiotensin II and endothelin-1 augment the vascular complications of diabetes via JAK2 activation. *Am. J. Physiol. Heart Circ. Physiol.* **293,** H1291–H1299 (2007).

118. Maffei, R. *et al.* Endothelin-1 promotes survival and chemoresistance in chronic lymphocytic leukemia B cells through ETA receptor. *PLoS One* **9,** e98818 (2014).

119. Ogata, Y. *et al.* Antiapoptotic effect of endothelin-1 in rat cardiomyocytes in vitro. *Hypertension* **41,** 1156–1163 (2003).

120. Ansley, D. *et al.* Propofol cardioprotection for on-pump aortocoronary bypass surgery (PRO-TECT II) - a Phase 2 randomized controlled trial. (2015). Manuscript submitted for publication.

121. Burgess, A. *et al.* Loss of human Greatwall results in G2 arrest and multiple mitotic defects due to deregulation of the cyclin B-Cdc2/PP2A balance. *Proc. Natl. Acad. Sci.* **107,** 12564–12569 (2010).

122. Chung, K. Y. & Walker, J. W. Interaction and inhibitory cross-talk between endothelin and ErbB receptors in the adult heart. *Mol. Pharmacol.* **71,** 1494–1502 (2007).

123. Chun, M., Liyanage, U. K., Lisanti, M. P. & Lodish, H. F. Signal transduction of a G protein-coupled receptor in caveolae: colocalization of endothelin and its receptor with caveolin. *Proc. Natl. Acad. Sci.* **91,** 11728–11732 (1994).

124. Wen, Z. & Darnell, J. E. Mapping of Stat3 serine phosphorylation to a single residue (727) and evidence that serine phosphorylation has no influence on DNA binding of Stat1 and Stat3. *Nucleic Acids Res.* **25,** 2062–2067 (1997).

125. Ogata, Y. *et al.* Antiapoptotic Effect of Endothelin-1 in Rat Cardiomyocytes In Vitro. *Hypertension* **41,** 1156–1163 (2003).

126. Chung, J., Uchida, E., Grammer, T. C. & Blenis, J. STAT3 serine phosphorylation by ERK-dependent and -independent pathways negatively modulates its tyrosine phosphorylation. *Mol. Cell. Biol.* **17,** 6508–6516 (1997).

127. Wen, Z., Zhong, Z. & Darnell, J. E. Maximal activation of transcription by Stat1 and Stat3 requires both tyrosine and serine phosphorylation. *Cell* **82,** 241–250 (1995).

128. Tian, Z. J. & An, W. ERK1/2 contributes negative regulation to STAT3 activity in HSS-transfected HepG2 cells. *Cell Res.* **14,** 141–147 (2004).

129. Van Harmelen, V. *et al.* Vascular peptide endothelin-1 links fat accumulation with alterations of visceral adipocyte lipolysis. *Diabetes* **57,** 378–386 (2008).

130. Harada, T. *et al.* Endothelin-1 activates extracellular signal-regulated kinases 1/2 via transactivation of platelet-derived growth factor receptor in rat L6 myoblasts. *Life Sci.* **104,** 24–31 (2014).

131. Mendoza, M. C., Er, E. E. & Blenis, J. The Ras-ERK and PI3K-mTOR pathways: Cross-talk and compensation. *Trends Biochem. Sci.* **36,** 320–328 (2011).

132. Ham, Y.-M. & Mahoney, S. J. Compensation of the AKT signaling by ERK signaling in transgenic mice hearts overexpressing TRIM72. *Exp. Cell Res.* **319,** 1451–1462 (2013).

133. Awasthi-Kalia, M., Schnetkamp, P. P. & Deans, J. P. Differential effects of filipin and methyl-beta-cyclodextrin on B cell receptor signaling. *Biochem. Biophys. Res. Commun.* **287,** 77–82 (2001).

134. Lambert, S., Vind-Kezunovic, D., Karvinen, S. & Gniadecki, R. Ligand-independent activation of the EGFR by lipid raft disruption. *J. Invest. Dermatol.* **126,** 954–962 (2006).

135. Zhuang, L., Lin, J., Lu, M. L., Solomon, K. R. & Freeman, M. R. Cholesterol-rich lipid rafts mediate Akt-regulated survival in prostate cancer cells. *Cancer Res.* **62,** 2227–2231 (2002).

136. Kabouridis, P. S., Janzen, J., Magee, A. L. & Ley, S. C. Cholesterol depletion disrupts lipid rafts and modulates the activity of multiple signaling pathways in T lymphocytes. *Eur. J. Immunol.* **30,** 954–963 (2000).

137. Rodal, S. K. *et al.* Extraction of cholesterol with methyl-beta-cyclodextrin perturbs formation of clathrin-coated endocytic vesicles. *Mol. Biol. Cell* **10,** 961–974 (1999).

138. Okamoto, Y., Ninomiya, H., Miwa, S. & Masaki, T. Cholesterol oxidation switches the internalization pathway of endothelin receptor type A from caveolae to clathrin-coated pits in Chinese hamster ovary cells. *J. Biol. Chem.* **275,** 6439–6446 (2000).

139. Paasche, J. D., Attramadal, T., Sandberg, C., Johansen, H. K. & Attramadal, H. Mechanisms of endothelin receptor subtype-specific targeting to distinct intracellular trafficking pathways. *J. Biol. Chem.* **276,** 34041–34050 (2001).

140. Boivin, B., Villeneuve, L. R., Farhat, N., Chevalier, D. & Allen, B. G. Sub-cellular distribution of endothelin signaling pathway components in ventricular myocytes and heart: Lack of preformed caveolar signalosomes. *J. Mol. Cell. Cardiol.* **38,** 665–676 (2005).

141. Lee, H. J., Chun, M. & Kandror, K. V. Tip60 and HDAC7 Interact with the Endothelin Receptor A and may be Involved in Downstream Signaling. *J. Biol. Chem.* **276,** 16597–16600 (2001).

142. Anderson, R. G. The caveolae membrane system. *Annu. Rev. Biochem.* **67,** 199–225 (1998).

143. Sandvig, K., Torgersen, M. L., Raa, H. A. & Van Deurs, B. Clathrin-independent endocytosis: From nonexisting to an extreme degree of complexity. *Histochem. Cell Biol.* **129,** 267–276 (2008).

144. Gonzalez, E. & McGraw, T. E. Insulin-modulated Akt subcellular localization determines Akt isoform-specific signaling. *Proc. Natl. Acad. Sci. U. S. A.* **106,** 7004–7009 (2009).

145. Hoeller, D., Volarevic, S. & Dikic, I. Compartmentalization of growth factor receptor signalling. *Curr. Opin. Cell Biol.* **17,** 107–111 (2005).

146. Smart, E. J. *et al.* Caveolins , liquid-ordered domains , and signal transduction. *Mol. Cell. Biol.* **19,** 7289–7304 (1999).

147. Heipieper, H. J., Keweloh, H. & Rehm, H. J. Influence of phenols on growth and membrane-permeability of free and immobilized Escherichia coli. *Appl. Environ. Microbiol.* **57,** 1213–1217 (1991).

148. Keweloh, H., Weyrauch, G. & Rehm, H. J. Phenol-induced membrane changes in free and immobilized Escherichia coli. *Appl. Microbiol. Biotechnol.* **33,** 66–71 (1990).

149. Compeer, M. *et al.* Agonist-dependent modulation of arterial endothelinA receptor function. *Br. J. Pharmacol.* **166,** 1833–1845 (2012).

150. Büther, K. *et al.* Assessment of endothelin-A receptor expression in subcutaneous and orthotopic thyroid carcinoma xenografts in vivo employing optical imaging methods. *Endocrinology* **153,** 2907–2918 (2012).

151. Macdonald, J. L. A simplified method for the preparation of detergent-free lipid rafts. *J. Lipid Res.* **46,** 1061–1067 (2005).

152. Asano, A. *et al.* Biochemical characterization of membrane fractions in murine sperm: Identification of three distinct sub-types of membrane rafts. *J. Cell. Physiol.* **218,** 537–548 (2009).